Synthesis and characterization of novel cathode materials for Li batteries and their applications in Li batteries

Dissertation for the Degree of Philosophiae Doctor (Ph.D.)

Pushpaka Bandara Samarasingha

Department of Chemistry

and

Centre for Materials Science and Nanotechnology

Faculty of Mathematics and Natural Sciences

University of Oslo

Norway

April 2015

Series of dissertations submitted to the
Faculty of Mathematics and Natural Sciences, University of Oslo
No. 1655

ISSN 1501-7710

Cover: Hanne Baadsgaard Utigard.
Printed in Norway: AIT Oslo AS.

Produced in co-operation with Akademika Publishing.

" This thesis is dedicated to those who always been there to share the laughter, happiness, tears, disappointment and frustration "

PREFACE

Since the day I learned about electrochemistry, I have been fascinated by the field and always wanted to learn more. After my Bachelor's Degree, I was fortunate enough to continue my Master's Degree on the field of lithium ion battery (LIB) cathode materials. When I finished my Master's Degree, I was looking for a place to pursue my doctoral studies. One of the offers I got was from the Chemistry department, University of Oslo (UiO), Norway. It included something I really enjoy doing, teaching which happened to be my favorite hobby. The position was in the field of LIB cathode materials. I did not have to think twice and accepted the offer. After moving to Norway, I began the endeavor to build a battery lab for bulk materials together with my fellow students who were focusing on thin film batteries. When I look back I feel happy that I was able to actively contribute with my experience to the process of building the battery lab from scratch and developing the test procedures here at the Chemistry department of UiO. Since then I have worked on LIB cathode materials (bulk). This thesis is the outcome of the research work and hence this is the first ever PhD thesis on bulk battery materials, performed here at the department of Chemistry, UiO.

I believe giving me the freedom to do my work according to my own plan and timetable, largely helped to successfully finish this work. I thank my supervisors, Prof. Helmer Fjellvåg and Assoc. Prof. Ola Nilsen, for giving me the freedom to do the work in my own way, for their assistance and advice during this work, from laboratory work to writing journal articles and this thesis. I thank the co-authors of research articles for their valuable contributions. From the Chemistry department, UiO, Oslo, Norway; Chris Thomas, Serena Margadonna, Jonas Sottmann, Niels Andersen and Susmit Kumar. Extended thanks to Jonas for supplying figures for in-situ synchrotron studies. From the Institute for Energy Technology, Kjeller, Norway; Magnus Sørby. From the Institute of Fundamental Studies (IFS), Kandy, Sri Lanka; Athula Wijayasinghe and Lakshman Dissanayake. Special thanks to Athula for the fruitful discussions, suggestions and friendly advice on a personal and academic level. From Department of Electrochemical Engineering, Royal Institute of Technology (KTH), Stockholm, Sweden; Göran Lindbergh and Mårten Behm. I acknowledge Prof. Yunhui Huang, Dean of School of Material

Science and Engineering, Huazhong University of Science and Technology (HUST), Wuhan, China; and his group for giving me the opportunity to work with his group and gain experience on battery research. David and Wojciech are warmly thanked for their assistance in XRD and Rietveld refinements. Sincere thanks to Karina B. Klepper for her assistance and cordial support given in making English language corrections of the thesis. I like to mention my first ever Master's Degree student, Ingunn Sandberg, for her friendly cooperation. I extend my thanks to all the NAFUMA group members and specially the battery group members; Knut, Ville, Vajeeston, Yang, Amund and Matthias for their cooperation and assistance. I would like to acknowledge UiO MILEN initiative (inter-faculty research area) and the department of Chemistry particularly for the award of the Research Fellowship which provided the necessary support for this research.

My heartfelt thanks to Karina, Mehdi, Media, Mari, Chris, Susmit, Maria, Kristin, Fabian and Per-Anders for sharing disappointment and frustration during evening tea, help when needed and the good times we enjoyed. Special thanks to Karina for introducing me to Norwegian cultural and social events and being there to give a friendly ear whenever I desperately wanted to talk to somebody. I am grateful to Jayakumar, Laurent and Titta, though they have left Norway long ago, for their help and support for my initial surviving phase after I arrived in Norway. I like to extend my thanks to Anne Eskild and her children (Hege, Aksel, Ingrid, Ellisiv, Susanne and Gunnar) for being nice to me and, providing a calm and quiet place to live during my over four years stay at their home.

I thank all my friends and colleagues in Norway, Sweden, China and Sri Lanka for their support and encouragement throughout, some of whom have already been named.

Last, but by no means least, I thank my loving mother, father, brothers, sister, brother-in-law, sister-in-laws and; nephews and nieces (Randika, Chalani, Damidu, Dilshan, Aakasha, Sanchalani and Siluni) for their care and love in all the time, though I have been far, far away from the home.

Pushpaka B. Samarasingha,
Oslo, Norway, April 2015.

TABLE OF CONTENT

Page

DEDICATION..... I

PREFACE..... III

TABLE OF CONTENT..... V

RESEARCH PUBLICATIONS..... IX

LIST OF TABLES..... XI

LIST OF FIGURES..... XIII

LIST OF ABBREVIATIONS..... XVII

Page

1. BASICS, PRINCIPLES AND THEORIES OF LITHIUM ION BATTERIES

1.1 Introduction..... 01

1.2 Primary batteries..... 02

1.3 Secondary Batteries..... 02

1.3.1 Nickel Cadmium Battery..... 03

1.3.2 Nickel Metal Hydride Battery..... 03

1.3.3 Lithium Ion Battery..... 04

1.4 The C- rate..... 05

1.5 Theoretical capacity of a material..... 06

1.6 Why Lithium ion batteries? 08

2. LITHIUM ION BATTERIES

2.1 Introduction..... 11

2.2 Origin of the Lithium Battery..... 12

2.3 Intercalation Concept..... 13

2.4 Origin of the Rechargeable Lithium ion Battery..... 14

2.5 Cathode materials for lithium ion battery..... 16
2.5.1 Exploration of Transition Metal Oxides as cathode materials..... 18
2.5.1.1 Oxides of Vanadium and Molybdenum..... 19
2.5.1.2 Lithium Cobalt Oxide, $LiCoO_2$ 20
2.5.1.3 Lithium Nickel Oxide, $LiNiO_2$..... 21
2.5.1.4 Lithium Manganese Dioxide, $LiMnO_2$..... 22
2.5. 1.5 Mixed Nickel-Manganese-Cobalt Dioxide, $Li(Ni_{1-y-z}Mn_yCo_z)O_2$ .. 23
2.5. 1.6 Spinels..... 23
2.5. 2 Lithium Iron Phosphate, $LiFePO_4$..... 25
2.6 Anode materials for lithium ion battery..... 27
2.7 Electrolytes..... 28
2.8 Nanomaterials..... 30

3. MATERIAL SYNTHESIS

3.1 Introduction..... 31
3.2 Methods used for synthesizing Lithium Ion Battery electrode materials.... 31
3.2.1 Hydrothermal Method..... 31
3.2.2 Mixed Hydroxide Method..... 32
3.2.3 Sol-gel process..... 33
3.2.4 Glycine-Nitrate Process..... 34
3.2.5 Pechini Method..... 35

4. THE PRESENT WORK..... 37

5. EXPERIMENTAL METHODS AND CHARACTERIZATION TECHNIQUES

5.1 Powder Synthesis..... 41
5.1.1 Spinel materials..... 41
5.1.2 New layered compounds based on $Li(Ni_{1/3}Mn_{1/3}Co_{1/3})O_2$ 42
5.1.3 Rutile and columbite structured materials..... 42
5.2 Powder characterization..... 43

5.2.1 X-ray diffraction..... 43
5.2.2 Neutron diffraction..... 43
5.2.3 Synchrotron experiments..... 44
5.2.4 Profile fitting and Rietveld analysis..... 44
5.2.5 Raman spectroscopy..... 45
5.2.6 Scanning electron microscopy (SEM)..... 45
5.3 Dense material (pellet) preparation and electrical characterization..... 45
5.4 Electrode fabrication and cell assembling..... 47
5.4.1 Electrochemical experiments..... 48

6. RESULTS AND DISCUSSION

6.1 Spinel phases (3D cathode materials)..... 51
6.1.1 In-situ XRD and X-ray absorption spectroscopy..... 53
6.1.2 Unpublished results on spinel materials..... 58
6.1.2.1 $LiNi_{0.5-x}Mn_{1.5+x}O_4$ (x = 0.1, 0.2)..... 58
6.1.2.2 Co substituted spinels..... 63
6.2 Layered NMC compositions (2D cathode materials)..... 65
6.3 Rutile and Columbite structured materials (1D cathode materials)..... 73

7. CONCLUDING REMARKS..... **79**

REFERENCES..... **82**

RESEARCH PUBLICATIONS

Spinel phases (3D cathode materials)

I. Neutron diffraction and Raman analysis of $LiNi_{0.5}Mn_{1.5}O_4$ spinel type oxides for use as lithium ion battery cathode and their capacity enhancements

Authors: Pushpaka B. Samarasingha*, Niels H. Andersen, Magnus Sørby, Susmit Kumar, Ola Nilsen, Helmer Fjellvåg.

Journal : **Manuscript.**

II. Detailed *in-situ* synchrotron study of ordered ($P4_332$) and disordered ($Fd\text{-}3m$) $LiNi_{0.5}Mn_{1.5}O_4$ spinel lithium ion battery cathode

Authors: Pushpaka B. Samarasingha*, Jonas Sottmann, Serena Margadonna, Ola Nilsen, Helmer Fjellvåg.

Journal : **Manuscript.**

Layered NMC compositions (2D cathode materials)

III. Development of cathode materials for lithium ion rechargeable batteries based on the system $Li(Ni_{1/3}Mn_{1/3}Co_{1/3-x}M_x)_2$, ($M$ = Mg, Fe, Al and x = 0.00 to 0.33)

Authors : Pushpaka B. Samarasingha*, Athula Wijayasinghe, Mårten Behm, Lakshman Dissanayake , Göran Lindbergh.

Journal : *Solid State Ionics*, **268 (2014) 226–230**, DOI - j.ssi.2014.07.012.

Rutile and Columbite structured materials (1D cathode materials)

IV. Investigation of Li^+ insertion in columbite structured $FeNb_2O_6$ and rutile structured $CrNb_2O_6$ materials

Authors **:** Pushpaka B. Samarasingha, Chris I. Thomas*, Helmer Fjellvåg.

Journal : *Electrochimica Acta*, **153 (2015) 232–237,** DOI - j.electacta.2014.12.004.

RESEARCH PUBLICATIONS - Author's contribution

Spinel phases (3D cathode materials)

I. Neutron diffraction and Raman analysis of $LiNi_{0.5}Mn_{1.5}O_4$ spinel type oxides for use as lithium ion battery cathode and their capacity enhancements

Planning and conducting the experiments (except Raman spectroscopy). Interpreting the data and writing the article

II. Detailed *in-situ* synchrotron study of ordered ($P4_332$) and disordered (Fd-3m) $LiNi_{0.5}Mn_{1.5}O_4$ spinel lithium ion battery cathode

Planning and conducting experiments, apart from the synchrotron related measurements. Interpreting data and heading the process of writing the article.

Layered NMC compositions (2D cathode materials)

III. Development of cathode materials for lithium ion rechargeable batteries based on the system $Li(Ni_{1/3}Mn_{1/3}Co_{1/3-x}M_x)_2$, ($M$ = Mg, Fe, Al and x = 0.00 to 0.33)

Planning and conducting the experiments. Interpreting the data and writing the article

Rutile and Columbite structured materials (1D cathode materials)

IV. Investigation of Li^+ insertion in columbite structured $FeNb_2O_6$ and rutile structured $CrNb_2O_6$ materials

Planning and conducting all the electrochemistry related experiments and interpreting related data. Conducting post galvanostatc experiment XRD and SEM. Taking part in writing the article

LIST OF TABLES

Page

Table 1.1 Theoretical capacities of popular LIB cathode materials..... 7

Table 4.1 Ionic radii of various cations..... 39

Table 5.1 Heat treatment of $LiNi_{0.5-x}Mn_{1.5+x}O_4$ materials..... 42

Table 5.2 Various compounds used as a binder and relevant solvents used..... 47

Table 6.1 Data based on electrochemical experiments of $LiNi_{0.5}Mn_{1.5}O_4$ / Li cells (1^{st} charge cycle)..... 52

Table 6.2 Structural parameters of the $LiNi_{0.5-x}Mn_{1.5+x}O_4$ powder materials based on PXRD (CuKα) data..... 60

Table 6.3 Discharge capacity values of the $LiNi_{0.5-x}Mn_{1.5+x}O_4$ powder materials obtained by galvanostatic experiments..... 63

Table 6.4 Comparison of first cycle charge capacity, first cycle discharge capacity and first cycle irreversible charge capacity of $Li(Ni_{1/3}Mn_{1/3}Co_{1/3-x}M_x)O_2$ (M = Fe, Al, Mg and x = 0.11, 0.22, 0.33) materials with those of $LiCoO_2$; charge and discharge rates C/5 (~ 36 mAh g^{-1}) 72

LIST OF FIGURES

Page

Figure 1.1 Cell voltage (V) vs. time (in hours) for the discharge of a rechargeable lithium ion battery at various constant currents..... 6

Figure 1.2 Ragone plots (Specific energy vs. specific power) for common rechargeable batteries..... 9

Figure 2.1 Schematic representation of a commercial lithium ion battery. Negative electrode (graphite), positive electrode ($LiCoO_2$), separated by a non-aqueous liquid electrolyte..... 11

Figure 2.2 Schematic illustration of $LiMO_2$ crystallographic structure (layered structure observed along (111) plane). The small green balls represent Li-ions..... 19

Figure 2.3 Potential vs. Li^+/Li profile of spinel $Li_xMn_2O_4$ for complete reversible lithium intercalation ($0 \leq x \leq 2$)..... 24

Figure 2.4 Unit cell structure of cubic spinel which depicts the site occupation; occupied sites (8a and 16d), unoccupied sites (16c)..... 25

Figure 2.5 Comparison of electrochemical stability of several LIB cathode materials relative to the electrochemical window of the electrolyte.... 29

Figure 3.1 The process flow chart of the Pechini technique..... 35

Figure 5.1 Setup used for the four probe electrical conductivity measurement, of pellet samples..... 46

Figure 5.2 Schematic diagram of the cross section of a 2032 coin cell..... 49

Figure 6.1 Results of galvanostatic charge discharge experiments of sample Mn15-900; inset depicts the results of rate tests in various specific currents..... 52

Figure 6.2 1^{st} charge curves of $LiNi_{0.5}Mn_{1.5}O_4$ / Li cells for 4.65-4.85 V range 53

Figure 6.3 Change of lattice constant with the capacity, (a) ordered material Mn15-900, (b) phase pure disordered material Mn15-600, (c) disordered material containing impurity..... 54

Figure 6.4 2D projection of in-situ XRD (λ = 0.50480 Å) patterns showing phase changes (a)ordered material Mn15-900 showing three phases, (b)phase pure disordered material Mn15-600 showing single phase, (c)disordered material containing impurity Mn15-900_60 showing two phases..... 55

Figure 6.5 In-situ XANE spectra (Ni K-edge) of sample Mn15-900 at maximal phase fraction showing $Ni^{2+}/Ni^{3+}/ Ni^{4+}$oxidation-recuction; solid line charge step, broken line discharge step..... 56

Figure 6.6 In-situ XANE spectra (Ni K-edge) after completed first charge step; (a) Mn15-600 beginning to end, (b) Mn15-600 compared to Ni^{3+} standard, $LaNiO_3$ (c) Mn15-600 compared to maximal phase fraction of phase II of sample Mn15-900, (d) Mn15-600 compared to end of charge step of sample Mn15-900 (e) Mn15-900_60 beginning to end, (f) Mn15-900_60 compared to Ni^{3+} standard, $LaNiO_3$..... 57

Figure 6.7 Powder X-ray diffraction (PXRD, CuKα) profiles of the $LiNi_{0.5-x}Mn_{1.5+x}O_4$ materials Sample information is given in the legends..... 59

Figure 6.8 Powder neutron diffraction profiles of the $LiNi_{0.5-x}Mn_{1.5+x}O_4$ materials..... 61

Figure 6.9 Indexed Superlattice related reflections of the $LiNi_{0.5-x}Mn_{1.5+x}O_4$ materials..... 61

Figure 6.10 SEM pictures of $LiNi_{0.5-x}Mn_{1.5-x}O_4$ materials. Sample information is given in the pictures..... 62

Figure 6.11 Powder X-ray diffraction (PXRD, CuKα) profiles of Co substituted spinel phases..... 64

Figure 6.12 Powder X-ray diffraction (PXRD, CuKα) profiles of substituted NMC compositions, $Li(Ni_{1/3}Mn_{1/3}Co_{1/3-x}M_x)O_2$ 66

Figure 6.13 Powder X-ray diffraction (PXRD, CuKα) profiles showing the impurity phase (*) and new phase (#) formed at the expense of layered structure..... 66

Figure 6.14 Electrical conductivity of $Li(Ni_{1/3}Mn_{1/3}Co_{1/3-x}Fe_x)O_2$..... 68

Figure 6.15 Electrical conductivity of $Li(Ni_{1/3}Mn_{1/3}Co_{1/3-x}Mg_x)O_2$..... 69

Figure 6.16 Electrical conductivity of $Li(Ni_{1/3}Mn_{1/3}Co_{1/3-x}Al_x)O_2$..... 69

Figure 6.17 SEM pictures of $Li(Ni_{1/3}Mn_{1/3}Co_{1/3-x}M_x)O_2$. Sample information is given in the pictures..... 70

Figure 6.18 PXRD (CuKα) of the columbite and rutile structured materials together with the reference patterns, star represents $Nb_{12}O_{29}$..... 74

Figure 6.19 Galvanostatic charge- discharge curves (1, 2, 5, and 10) of $CrNb_2O_6$ (Cr-S1); P1, P2, P3 - discharge plateaus..... 75

Figure 6.20 Cyclic voltammograms of $CrNb_2O_6$ (Cr-S1)..... 76

Figure 6.21 SEM micrographs of (a)Cr-S1, (b)Fe-S1and (c)Fe-S2..... 77

LIST OF ABRIVIATIONS

E_{cell}	Theoretical voltage of a cell
E	Voltage
I	Current
NiCad or Ni|Cd	Nickel cadmium battery
Ni|MH	Nickel-metal hydride battery
LIB	Lithium ion battery
NMP	n-methylpyrrolidone
PTFE	Polytetrafluoroethylene
PVDF	Polyvinylidene fluoride
PVDF-HFP	Poly(vinylidene fluoride-*co*-hexafluoropropylene)
EG	Ethylene glycol
CA	Citric acid
PC	Propylene carbonate
EC	Ethylene carbonate
DEC	Diethyl carbonate
ALD	Atomic layer deposition
GNP	Glycine nitrate process
CVD	Chemical vapour deposition
PVD	Physical vapour deposition
PXRD	Powder x-ray diffraction
PND	Powder neutron diffraction
XAS	X-ray absorption spectroscopy

1. BASICS, PRINCIPLES AND THEORIES OF LITHIUM ION BATTERIES

1.1 Introduction

The Italian physicist Alessandro Volta (1745-1827) can be credited for the invention of the modern battery in 1800 [1]. He described an assembly consisting of plates of two different metals, such as Zn and Cu, which were placed alternately in a stack-like manner. The plates were separated by a piece of paper soaked in an aqueous solution, such as brine or vinegar. If the ends of the assembly were touched, it was capable of producing an electrical shock to whomever touched it. The battery described by Volta was a compilation of several electrochemical cells. In a broad sense, they could be defined as a device that converts chemical energy into electrical energy. Since this invention, the battery has been developed into a more practical device. It is now a common power supply device for a vast range of applications, from consumer electronics to electrical vehicles.

The present common term "battery" consist of single (though the term "battery" means a collection), or multiple galvanic cells, connected in series or parallel to generate higher voltages or higher currents, respectively. Each such cell consists of two electrodes: The anode where the oxidation reaction takes place during discharge and the cathode where the reduction takes place. In commercial batteries, they are called negative and positive electrodes, respectively. The theoretical voltage[1] of a cell, $E_{cell,}$ is governed by the nature of the chemical reactions at the two electrodes. The power it can deliver, defined as the product of the voltage (E) and the current (I), is governed by much more trivial factors, such as the electronic and ionic conductivity of the active materials, the stability of the interfaces between different parts, solution decomposition in the electrolyte [2,3].

[1] *Though the voltage is a measure of the electrochemical potential of an electrochemical cell, voltage/electrochemical potential/cell potential/ cell voltage are conventionally used as synonyms. The same convention is used in this thesis as well*

Batteries can be broadly divided into two categories, namely, primary batteries and secondary batteries depending on whether or not they can be charged. The primary batteries are not meant to be recharged, while the secondary batteries are built for multiple charging cycles.

In following sections, the chemistry of three common portable rechargeable batteries and two important concepts associated with the batteries, the C rate and theoretical capacity, are discussed. Furthermore, the reason why lithium ion batteries are important compared to other rechargeable batteries is also discussed.

1.2 Primary batteries

In primary batteries, the spontaneous exothermic cell reaction that takes place while a current is drawn, is not practically reversible, and hence are not meant to be recharged. The Leclanché battery (Zn|MnO_2 dry cell), aluminum-air battery, mercury oxide battery, silver oxide battery and zinc-air battery are all examples of popular primary batteries. Since the focus of the current thesis is on secondary batteries, the chemistry behind the primary batteries will not be dealt with any further.

1.3 Secondary Batteries

Secondary batteries are based on reversible chemistries and are constructed with the aim of sustaining multiple (dis)charging cycles. Three types of commonly known portable secondary batteries are the nickel cadmium (Ni|Cd), nickel metal hydride (Ni|MH) and lithium-ion batteries (LIB). The Ni|Cd system has presently lost a large portion of its market to the Nickel-metal hydride and lithium ion batteries. However, despite this, the Ni|Cd system still prevails as a rechargeable battery system in such devices as portable communications equipments, portable hand tools and appliances and radio control modules.

1.3.1 Nickel Cadmium Battery

Nickel cadmium batteries [2,3] are known to be the first rechargeable batteries for power tools and portable electronics, $E_{cell} \sim 1.2$ V. Nickel cadmium is commonly abbreviated as NiCad or Ni|Cd. The principal advantages of Ni|Cd over other rechargeable types are good charging efficiency, small variation in terminal voltage during discharge, low internal resistance, and non-critical charging conditions. They can replace regular batteries in most applications. The Ni|Cd cell contains a nickel hydroxide positive electrode plate, a cadmium negative electrode plate, a separator and an alkaline electrolyte.

The positive electrode reaction:- $2NiO(OH) + 2H_2O + 2e^- \underset{\text{charge}}{\overset{\text{discharge}}{\rightleftharpoons}} 2Ni(OH)_2 + 2OH^-$

The negative electrode reaction:- $Cd + 2OH^- \underset{\text{charge}}{\overset{\text{discharge}}{\rightleftharpoons}} Cd(OH)_2 + 2e^-$

The overall cell reaction is, $2NiO(OH) + Cd + 2H_2O \leftrightarrow 2Ni(OH)_2 + Cd(OH)_2$

The Ni|Cd system is expected to become totally displaced by the nickel-metal hydride and lithium ion batteries, due to the hazardous nature of Cd, which has raised major environmental concerns.

1.3.2 Nickel Metal Hydride Battery

The nickel-metal hydride battery [2,3], which is abbreviated as Ni|MH with $E_{cell} \sim 1.2$ V, is a popular rechargeable system similar to nickel-cadmium (Ni|Cd) battery but using a hydrogen-absorbing alloy for the negative electrode instead of cadmium. Its active cathode material is nickel hydroxide, $Ni(OH)_2$, which has a layered crystal structure. The anode, denoted as MH, consists of an alloy incorporating an array of mainly rare earth elements. During charging, the nickel in $Ni(OH)_2$ undergo oxidation to yield NiOOH The

anode reduces water to elemental hydrogen, which combines with the metal to form a hydride, the same process as in hydrogen storage.

The negative electrode reaction: - $H_2O + M + e^- \underset{\text{discharge}}{\overset{\text{charge}}{\rightleftharpoons}} OH^- + MH$

The positive electrode reaction: - $Ni(OH)_2 + OH^- \underset{\text{discharge}}{\overset{\text{charge}}{\rightleftharpoons}} NiO(OH) + H_2O + e^-$

The overall cell reaction is, $Ni(OH)_2 + M \leftrightarrow NiOOH + MH$

The NiMH system seemingly has gained its highest market share at present. This system is expected to retain a solid market share for many years as NiMH batteries are still preferred for large scale production of equipments where high power is needed, for example power tools.

1.3.3 Lithium Ion Battery

Lithium-ion batteries [2-5], commonly abbreviated as LIB, are a type of rechargeable batteries in which the lithium ion moves between the anode and the cathode through intercalation processes. The lithium ion moves from the anode to the cathode during discharge and from the cathode to the anode when charging. This gives rise to a mechanism widely known as the rocking chair mechanism.

The negative electrode reaction: - $C + xLi^+ + xe^- \underset{\text{discharge}}{\overset{\text{charge}}{\rightleftharpoons}} CLi_x$

The positive electrode reaction: - $LiCoO_2 \underset{\text{discharge}}{\overset{\text{charge}}{\rightleftharpoons}} Li_{1-x}CoO_2 + xLi^+ + xe^-$

The overall cell reaction is,

$$LiCoO_2 + C \leftrightarrow Li_{1-x}CoO_2 + CLi_x$$

A detailed discussion on lithium ion batteries is given in chapter 2.

When comparing the above mentioned battery technologies, NiCd and NiMH have reached the optimum development, and NiCd system is approaching its end of the battery market.

The lithium ion battery technology is meanwhile still under development. At present, the lithium ion battery technology consists of a couple of such sub technologies as; conventional lithium ion batteries, lithium polymer batteries, lithium sulphur batteries and lithium air batteries. Lithium ion and lithium polymer batteries have already reached the market despite the need for further development. However, none of these battery technologies are perfect. They suffer from various draw backs associated with cathode, anode, electrolyte and interfaces. Therefore, there is a huge potential and need for research devoted to the development of lithium ion battery technology at present. This thesis focuses on conventional lithium ion battery technology and here after "lithium ion battery" is used in that sense.

1.4 The C-rate

One important concept when comparing the above mention battery systems, NiCd, NiMH and LIB, is how fast these batteries can be discharged (and charged). Battery manufactures often prefer to express discharge rates in units of C (one should not confuse with the symbol used for Coulomb). In this scale, C/10 (or 0.1C) corresponds to the current at which the useful practical capacity of the battery is consumed in 10 h. Figure 1.1 shows the discharge profiles for a rechargeable lithium ion battery with $Li(NiMnCo)_{1/3}O_2$ as the cathode material. The potential of the battery is monitored for different discharging rates (I = 0.25 to 5 mA, i.e. 10 to 0.5 h, respectively). As the C rate is increased beyond a certain limit, the full capacity of the battery can no longer be utilized. This is clearly illustrated by curve Z in Figure 1.1, where the lifetime falls short of the 0.5 h predicted based on the results obtained at the lower C rates. A fraction of valuable electrode material remained unused, and this effect is found for all battery systems for

sufficiently high C rates. This is one of the challenges material scientists and engineers face when developing highly efficient battery technologies. To address this challenge, a deep understanding of the underlying processes involved are required. However the main problem is almost always linked to hindrances in the transport of charged species [2,5,6].

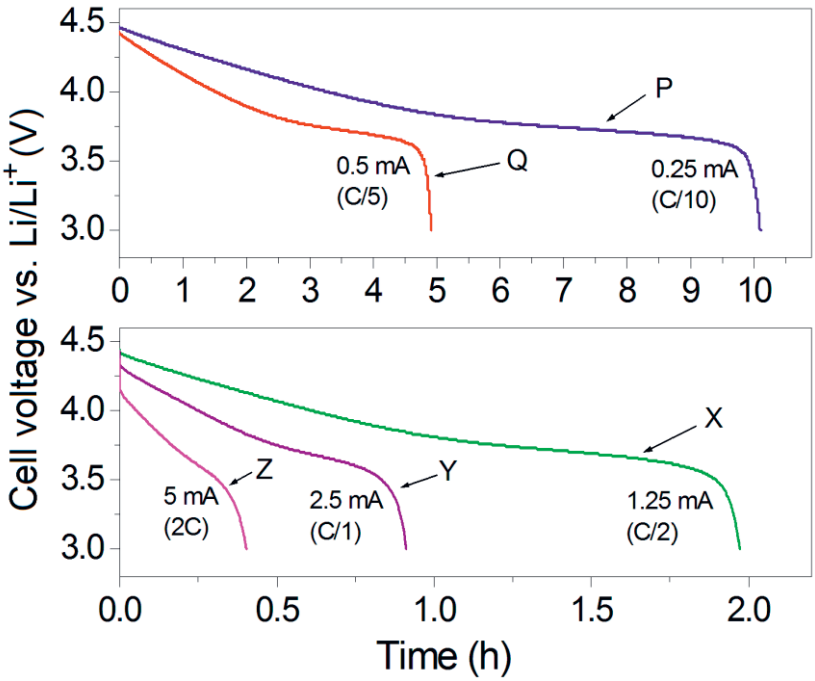

Figure 1.1 *Cell voltage (V) vs. time (in hours) for the discharge of a rechargeable lithium ion battery at various constant currents (i.e. at various C rates).*

1.5 Theoretical capacity of a material

In the previous section, limitations related to practical capacity was raised. Provided that none of these limitations are present, the capacity of a battery is determined by its chemistry. The capacity calculated assuming a complete chemical reaction that takes place at the cathode is known as the theoretical capacity. The following equation

describes the relationship between the theoretical specific capacity ($C_{theoretical}$) and the molar mass of a cathode material.

$$C_{theoretical}\ (mAh\ g^{-1}) = \frac{nF}{M_r} \times \frac{1}{3.6} \qquad (1.1)$$

where, *n* is the number of moles of electrons (or the number of moles of Li^+ in one mole of the compound), *F* is the Faraday constant (F = 96,485 s A / mol) and M_r is the molar mass of the cathode material in its discharge state. Table 1.1 gives the $C_{theoretical}$ values of some prominent cathode materials calculated using equation 1.1.

Table 1.1 Theoretical capacities of popular cathode materials for lithium ion battery.

Compound	**n**	**M_r (g/mol)**	**$C_{theoretical}$ (mAh g^{-1})**
$LiCoO_2$	1	97.87	274
$LiMn_2O_4$	1	180.82	148
$Li_2Mn_2O_4$	2	187.76	286
$LiNi_{0.5}Mn_{1.5}O_4$	1	182.69	147
$Li(Ni_{1/3}Mn_{1/3}Co_{1/3})O_2$	1	96.40	278
$LiFePO_4$	1	157.75	170

Using the theoretical capacity of a material and the voltage of the cell, it is possible to derive other important terminologies associated with battery technology such as specific power, specific energy. In the following section, these concepts are discussed. For example, if all the lithium in $LiCoO_2$ is extracted, the cell voltage vs Li/Li^+ becomes 4.7 V. Then the theoretical specific energy can be calculated as follows.

$$specific\ energy = \frac{cell\ voltage\ (V) \times current\ drawn\ (A) \times time(h)}{mass\ active\ material\ (kg)} \qquad (1.2)$$

$$= cell\ voltage\ (V) \times theoretical\ capacity = 4.7V \times 274\frac{Ah}{kg}$$

$$= 1288\ Whkg$$

In comparison, the theoretical specific gravimetric energy density of the $LiCoO_2$ cathode (1,288 Wh/kg) is almost 10 times less than that of gasoline (ca. 12,000 Wh/kg). Therefore, it is unrealistic to think that gasoline would be totally replaced by lithium ion battery technology in transportation, though they are already used in electric and hybrid vehicles.

1.6 Why Lithium ion batteries?

Selection of a particular battery for a specific device is often made primarily based on its performance characteristics. One such characteristic is obtained by extracting a constant current, while monitoring cell voltage as a function of time. Shown in Figure 1.1 is a plot of cell voltage vs. time for various discharge currents for a rechargeable lithium ion battery (based on the work mentioned in ref. 4). As depicted in Figure 1.1, for *I* = 0.25 mA (see curve P), *E* decreases slowly during the first 5 h to reach a fairly constant plateau. After about 10 h, *E* drops suddenly and very rapidly indicating the end of the battery's useful life for that discharge cycle. Based on the observed lifetime, the charge (or capacity) the battery can deliver under these conditions is:

$$10h \times 3600\frac{s}{h} \times 0.00025A = 9\ coulombs$$

In battery technology units, this is equal to 2.5 mAh (0.25 mA × 10 h). If the current is increased to meet the demands of a more power consuming device, for example, the observed useful life of the battery is obviously shorter. This is illustrated by the curve Q in Figure 1.1 for *I* = 0.5 mA. Nevertheless, based on the same calculation presented above, the capacity of the battery remains virtually unchanged i.e. 2.5 mAh, (0.5 mA × 5

h). However, when the values relevant to curve Z are considered, the practical useful capacity is lower, i.e. 2.0 mAh (5 mA x 0.4 h).

A useful means of representing the operational performance of batteries and other energy storage and energy conversion devices is a graphical representation of specific energy (described by equation 1.2) vs. specific power (W/kg). This graph is known as a Ragone plot, and examples for common rechargeable battery types are shown in Figure 1.2.

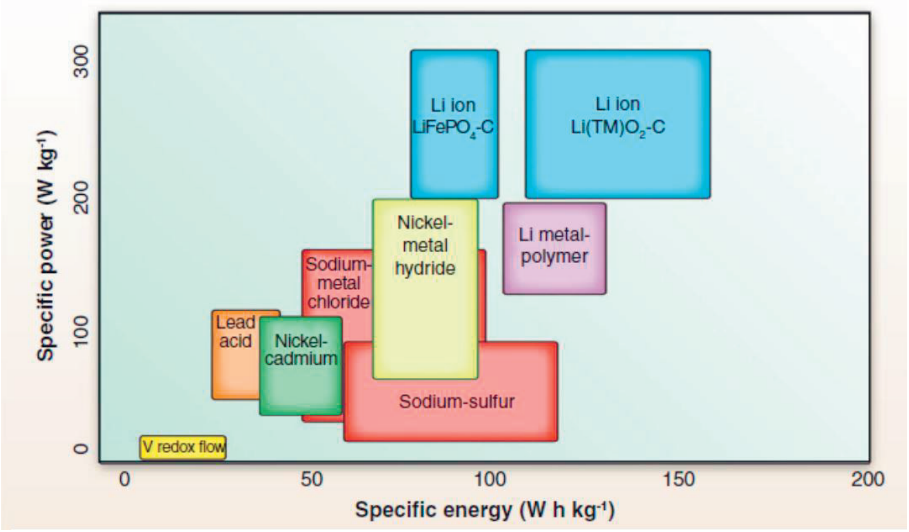

Figure 1.2 *Ragone plots (Specific energy vs. specific power) for common rechargeable batteries [7].*

It is obvious from Figure 1.2, that the lithium ion battery has twice the specific energy compared to the nickel metal hydride battery and four times that of nickel cadmium battery for a given specific power. Although specific energy and specific power are important parameters, other factors such as reliability, safety, self-discharge, operating temperature, and even the effect of humidity, must also be considered when choosing a battery system for a specific application. Other major concerns today are the effect on

the environment and health hazards not only during the operation lifetime of a battery, but also after its disposal.

Lithium ion batteries are today's leading power source for portable electronics. From an overall perspective they indisputably represent the most promising energy storage system for a number of other applications, including transportation. Hence, certain aspects of its principles of operation deserve particular attention. This will be dealt with in Chapter 2.

2. LITHIUM ION BATTERIES

2.1 Introduction

Rechargeable Lithium ion batteries consist of a positive electrode (cathode), Li ion containing electrolyte and negative electrode (anode), Figure 2.1.

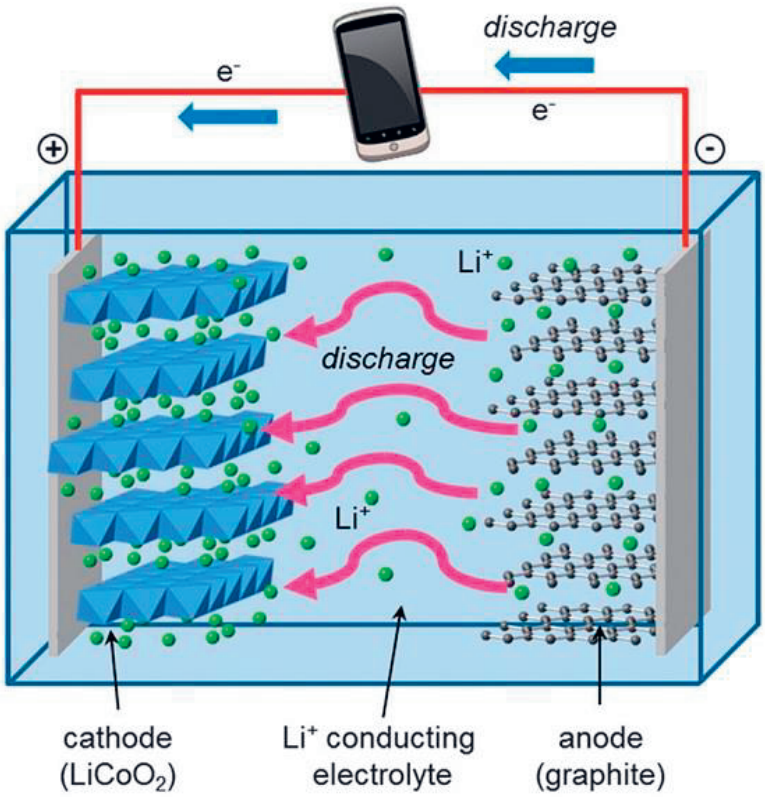

Figure 2.1 *Schematic representation of a commercial lithium ion battery. Negative electrode (graphite), positive electrode ($LiCoO_2$), separated by a non-aqueous liquid electrolyte [8].*

When transition metal oxides, such as $LiCoO_2$, was first introduced as the cathode in lithium ion battery, metallic lithium was used as the anode material. This battery had an $E_{cell} \sim 4.7$ V. The commercial electrodes of lithium ion batteries are made of micron size

particles of graphite (anode) and $LiCoO_2$ (cathode), mixed with relatively high surface area carbon as a conductivity enhancer, as well as an organic binder to provide structural integrity. A schematic representation of the charge and discharge processes associated with the operation of a commercial lithium ion battery is shown in Figure 2.1.

Both $LiCoO_2$ and graphite are Li ion insertion hosts. During the charging process, Li ions are extracted from the $LiCoO_2$ electrode and inserted into the graphitic carbon electrode, coupling with negatively charged electrons to keep the overall charge balance. During the discharging process, Li ions are reversibly extracted from the negative electrode and inserted into the positive electrode. This process led to the coining of such terms as rocking chair or shuttlecock to describe more literally its mode of operation. The electrochemical insertion/extraction process is a solid-state red-ox reaction in the host material. It involves an electrochemical charge transfer coupled with the insertion/extraction of mobile guest ions into/from the structure of an electronic and ionic conductive solid host. The major structural features of the host are kept after the insertion/extraction of the guests.

2.2 Origin of the Lithium Battery

The term "Lithium battery" was commonly used to identify primary lithium batteries. The concept first originated from Japan [9]. The first cell developed was the $Li/(CF)_n$ battery. This was developed by the Panasonic corporation (then Matsuhita electric industries) [9,10]. Lithium fluoride and carbon are considered to be the end products of this battery chemistry. However, considering the cell potential of 2.8 - 3.0 V of this cell Whittingham [9,11] proposed that lithium initially intercalates the carbon mono-fluoride lattice and subsequently the lithium fluoride is formed according to the following reaction sequence.

$$x\text{Li} + (\text{CF})_n \rightarrow \text{Li}_x(\text{CF})_n \rightarrow \text{C} + \text{LiF}$$

Although much work was carried out on the carbon fluorides, the major challenge has been to make this reaction reversible, even for lower fluoride levels [9]. Lithum-

sulphurdioxide (Li/SO_2), lithium-thionyl chloride ($Li/SOCl_2$), lithium-manganese dioxide (Li/MnO_2), lithium-copper oxide (Li/CuO), lithium-silver vanadium oxide ($Li/Ag_2V_4O_{11}$) are some of the other types of primary lithium batteries. Li/MnO_2, which is one of the first generation lithium batteries, was developed by the SANYO Corporation. Even though they initially sold this battery for solar rechargeable calculators, the battery is used in many other electronic devices today. The $Li/Ag_2V_4O_{11}$ cell has been used in implantable medical devices for a long time, for example in cardiac defibrillators [12,13]. This cell has been preferred mainly due to two reasons: Firstly, metallic silver is formed during discharge, which greatly improves the electronic conductivity; secondly, more than one lithium can combine with vanadium, which leads to a capacity over 300 mAh g^{-1}. Wu *et al* [14] has recently reported improved properties of this battery system. For future implantable medical devices, "Biological fuel cells" have been proposed as an alternative to the lithium batteries. These devices can extract "fuel", for example glucose, directly from the blood stream. However, this concept is currently far from application. Therefore, rechargeable battery systems are needed to power such medical devices.

2.3 Intercalation Concept

Early concepts of intercalation, also known as the rocking chair mechanism, reportedly originated during the early 1970ies. The concept was based on placing an electrochemically active species (ions/molecules) inside a host material. The first such study was intercalating iodine or sulphur in a dichalcogenide host material [15]. Broadhead *et al* [15] holds the patent describing this concept for a rechargeable non-aqueous battery. They describe materials such as $TaTe_2$, TaS_2, WS_2, WSe_2, WTe_2, $MoSe_2$, $MoTe_2$, NbS_2, $NbSe_2$, $NbTe_2$, TiS_2 and $TiTe_2$ as host dichalcogenide materials. They also describe that the dichalcogenide host itself was electrochemically inert [16]. Another such effort to study intercalation was by trying to insert oxides and halides in between graphite layers [9,17,18]. However, further studies revealed that there were no intercalation but rather a mixture of oxide/halide and graphite was produced. Whittingham [9] describes C_8K and C_8Br as possible intercalation compounds where K

and Br would reversibly intercalate in to graphite. However, this concept has not still been tested. Gunst *et al* [19] have tested de/intercalation of Cu in TaS_2 and $TiSe_2$ single crystals.

The most successful and simple intercalation among the studied processes was lithium intercalation in TiS_2. This pioneering work was carried out by Whittingham for the Exxon company and hence he holds the patent for chalcogenide battery describing this concept [20]. Whittingham described that a drop in the free energy is expected with increasing amount of lithium intercalation. This is due to two reasons; firstly, repulsive interactions between the like charges (Li^+) are increased with increasing lithium content, secondly, electrons combining with TiS_2 must occupy continuously increasing energy levels [20]. However, there is very little change in the free energy with temperature, as is usually expected for a solid-state reaction. This fact coupled with the high lithium ion diffusivity and the electronic conductivity of TiS_2 makes the Li/TiS_2 couple ideal for energy storage. An efficiency of > 90% is expected for this couple. The amount of energy that can be stored in this system is 480 Wh/kg based on the active material mass. However, this is much less than what is stored in an equal mass of gasoline, ca. 12,000 Wh/kg.

2.4 Origin of the Rechargeable Lithium ion Battery

As mentioned under the section 2.3, during the early 1970ies researchers discovered that a range of electron-donating molecules and ions could be intercalated into layered dichalcogenides. Among them some compounds got attention for their material properties, for example TaS_2 was interesting for superconductivity studies [17,21,22]. However, most of the materials were studied for energy storage purposes. In this group, TiS_2 was considered to be the most attractive compound as a battery electrode. Moreover, it was the lightest among all the layered dichalcogenides, meaning it had the highest gravimetric energy density [16,20,21,23]. Thompson discovered that it was a semi-metal, which therefore eliminated the need of a conductive additive to construct the cathode [24]. Meanwhile, Whittingham revealed that the material was stable for all

stages of lithium insertion and it remained as a single phase during the reaction $Li^+ + TiS_2 \rightarrow LiTiS_2$ [21,25]. Because of this single-phase reaction, not only all the lithium can be reversibly intercalated but also it eliminates the energy wasted for nucleation and rearrangements of new phases which otherwise would occur for binary phase reactions. A binary phase system may also cause problems for the stability of the cathode structure. In comparison, the leading cathode material for today's lithium ion battery, $LiCoO_2$, suffer from irreversible phase changes upon complete removal of Li. Hence, only half of the Li can be reversibly removed, which reduces its overall capacity notably. Even though the amount of Li that can be reversibly removed has presently been improved to 2/3 by substituting Co with Mn and Ni, this is still far from utilizing one lithium per transition metal atom. These dichalcogenides, specially disulfides, are also interesting materials for sodium ion batteries [3,6,9].

Tri-chalcogenides were next in line to be studied as host materials for lithium intercalation. Niobium triselenide was one of the first such materials investigated and reported to reversibly intercalate three lithium ions to form Li_3NbSe_3 [26,27]. Even though, other tri-chalcogenides were also studied, they did not reversibly react with lithium ions like $NbSe_3$. For example, TiS_3 was studied and found to react to form Li_2TiS_3 through a two phase reaction. It was suggested that the S-S bond in TiS(S-S) is broken during the first lithium insertion. During the second lithium intercalation, Ti^{4+} is reduced to Ti^{3+} , in a similar way as in TiS_2. This makes only one lithium ion can be reversibly intercalated into TiS_3, just as in TiS_2 [28]. Even though other chalcogenide materials having a high theoretical capacity have been studied, they have not received much interest. This is mainly due to poor rate capabilities or low conductivity [3,6,9].

Another class of materials having the same structure as layered dichalcogenides, the layered oxides, was ignored during the early 1970ies as lithium intercalation host materials beside its structural similarity. This is surprising given the extent for which oxides were studied, but at the time researchers thought these oxides would not

reversibly intercalate lithium. Moreover, thermal stability problems and safety concerns regarding oxides towards the right side of the periodic table deferred studies of them as lithium intercalation hosts [3,6,9]. These oxides got their attention through the studies of Goodenough in the late 1970ies. Through these studies, the next class of lithium intercalation materials emerged. They have proven to become the dominant lithium ion battery cathodes at present [3,8,9].

2.5 Cathode materials for the lithium ion battery

The key requirements for a material to be successful as the cathode of a rechargeable lithium battery are as follows, after Whittingham [9]:

(1) The material should contain a readily reducible/oxidizable ion, for example a transition metal.

(2) The material should react with lithium in a reversible manner.
This denotes an intercalation-type reaction in which the host structure essentially does not change as lithium is added.

(3) The material should react with lithium with a high free energy of reaction.
    (a) High capacity, preferably at least, one lithium per transition metal.
    (b) High voltage, preferably around 4 V (as limited by stability of electrolyte).

(4) The material should react with lithium very rapidly both on insertion and removal.
This leads to high power density.

(5) The material should be a good electronic conductor, preferably a metal.
    (a) This allows for the easy addition or removal of electrons during the electrochemical reaction.
    (b) This allows for reaction at all contact points between the cathode active material and the electrolyte rather than at ternary contact points between the cathode active material, the electrolyte, and the electronic conductor (such as carbon black).

(c) This minimises the need for inactive conductive diluents, which reduce the overall energy density.

(6) The material should be stable, i.e., does not change structure or otherwise degrade, to over-discharge and overcharge.

(7) The material should be of low cost.

(8) The material should be environmentally benign.

However, at present there is no single lithium ion battery cathode material totally fulfilling above criteria. For example, the prime cathode material for commercial lithium ion battery, $LiCoO_2$, is capable of extracting only half of the available Li. This is below par from the expectation of one Li per transition metal. Furthermore, there is a need of addition of conductive additive due to the low electronic conductivity of the oxide. Thermal stability problems associated with the material is another major concern with $LiCoO_2$. Moreover, Cobalt is expensive and toxic, and hence an obstacle for the implementation of this material into mass production of cheap and reliable portable power sources. Some of the main challenges lithium ion battery researches face :

a) Achieving reversible extraction of one lithium per transition metal,

b) Increasing the electrical conductivity,

c) Discover and explore thermally more stable materials,

d) Discover and explore materials with higher potential vs. Li/Li^+,

e) Discover and explore materials with higher rate capability,

In the following sections lithium ion battery cathode materials, anode materials and electrolytes are discussed.

2.5.1 Exploration of Transition Metal Oxides as cathode materials

The discovery of transition metal oxides, LiMO_2, for use as the reversible lithium ion battery cathode was done by Goodenough in the 1970s. These materials displayed very positive operating potentials. In particular, $LiCoO_2$ proved to be key in the development and commercialization of secondary lithium ion batteries by SONY Corporation, Japan as power sources for many of their own electronic devices [3,7,9].

In this class of compounds represented by LiMO_2, the octahedral sites in a cubic close-packed oxygen array are occupied by transition metal ions (*M*) and lithium ions. Moreover, the lithium layers lie between the slabs of octahedra formed by *M* and oxygen atoms. The materials having such a structural arrangement are called layer structured materials [3,5,6,9,29], as shown in Figure 2.2. The electrochemically active species in these materials, *M*, is typically a transition metal such as cobalt, manganese or nickel. The average oxidation state of the *M* cation in LiMO_2 is +3. The electrochemical reaction which takes place can be represented as follows, after He *et al* [29]:

$$\underset{(oct)}{Li}\ \underset{(oct)}{M}\ \underset{(cp)}{O_2} \underset{\text{discharge}}{\overset{\text{charge}}{\rightleftharpoons}} \underset{(oct)}{\square}\ \underset{(oct)}{M}\ \underset{(cp)}{O_2} + Li$$

where (oct) stands for the octahedral sites in a close packed oxygen array denoted by (cp) while □ represents the octahedral voids (blank sites). Li ions in the Li layer are considered to be mobile from one octahedral site to another [9,29]. In other words, layer structured intercalation materials provide a two dimensional interstitial space. This can facilitate fast Li ion mobility in the host materials. The ease of movement for Li ion in a layered structure is considered to be an important advantage in terms of Li ion diffusion compared to one dimensional tunnel structured materials such as rutile, columbite and olivine. These materials encounter limited Li ion bulk diffusion [9,29]. Rutile and columbite structured materials and Li intercalation in these materials are discussed further in paper IV.

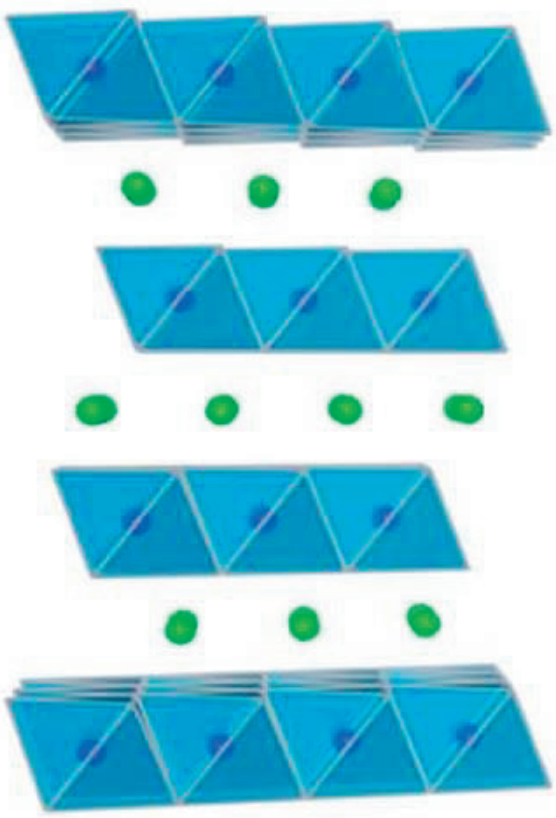

Figure 2.2 *Schematic illustration of $LiMO_2$ crystallographic structure (layered structure observed along (111) plane). The small green balls represent Li-ions [29].*

2.5.1.1 Oxides of Vanadium and Molybdenum

Two of the oxides which were studied earliest as lithium intercalation materials are vanadium and molybdenum oxides. These oxides were derived from their respective highest oxidation states, V_2O_5 and MoO_3. Although molybdenum trioxide is capable of intercalating ca 1.5 lithium per molybdenum, it was of less interest due to its low rate capability [9,30]. However, recently Wang *et al* [31] have shown that with the introduction of nitrogen to the structure in the form of nitride ions, the rate capability

was greatly improved. The capability is enhanced due to increased conductivity in the MoO_3 nano belts. V_2O_5 is a layered structure material which has weak bonds between the layers. It has been studied for decades and reported to reversibly react with lithium by a intercalation reaction mechanism as shown below [9,74,32]:

$$x\text{Li} + V_2O_5 \leftrightarrow \text{Li}_xV_2O_5$$

This intercalation mechanism involves several phase changes and is rather complex [3,7,9]. Other vanadium oxides with various oxidation states of vanadium and with different structures have also been studied. LiV_3O_8 is one such oxide [9].

2.5.1.2 Lithium Cobalt Oxide, $LiCoO_2$

As mentioned under section 2.5.1, Goodenough realized what potential $LiCoO_2$ had as a lithium ion battery cathode material. $LiCoO_2$ also has a layered structure similar to TiS_2. , Meanwhile Whittingham was studying dichalcogenides as lithium ion battery cathode materials [3,5,6,9]. $LiCoO_2$ has a well known α-$NaFeO_2$ layered structure with R-3m space group. Moreover, it has a very promising cell voltage upon complete removal of lithium, 4.7 V *vs.* Li/Li^+, and a theoretical capacity of 274 mAh g^{-1}. Thus, the gravimetric energy density is as high as 1288 Wh/kg. These are very attractive figures for a lithium ion battery cathode. However, irreversible structural changes occur while trying to extract all the lithium from $LiCoO_2$ [33-35]. As a result, only half of the lithium can be reversibly extracted from $LiCoO_2$. Consequently, the practical capacity is limited to 137 mAh g^{-1} and the voltage to 4.2 V *vs.* Li/Li^+. However, Amatucci *et al* [36] have reported that they have successfully isolated CoO_2 for the first time and 95% lithium reinserted without reported structural changes. Nevertheless, they have carried out electrochemical testing using dry plastic lithium ion battery technology [36]. Several different phases have been reported to exist in the range between $LiCoO_2$ and CoO_2. Rossen *et al* [37] report formation of $Li_{0.5}CoO_2$ in the spinel form. Even though this composition has not been reported to form during lithium de/intercalation, Gabrisch *et al* [38] observed traces of the spinel phase on the surface of the extensively cycled $LiCoO_2$.

In 1991 the SONY Corporation combined $LiCoO_2$ cathode with a carbon (graphite) anode to make the first successful commercial lithium ion battery [3,5,9,39,40], which still dominates the lithium battery market. The battery was produced with the cathode in the discharged state. This was a turning point for lithium ion battery research. Until this time, researchers thought the cathode should be in the charged state to be used in lithium ion battery. The use of graphitic carbon as anode results in the loss of 100-300 mV in cell potential. Even though this loss is feasible with the higher potential of the $LiCoO_2$ cathode, it was not favourable for the lower potential of the TiS_2 cathode. Moreover, the carbon anode, which forms the compound LiC_6 on reaction with lithium, proved to make the battery much safer than by use of lithium alone. However, some practical concerns such as limited availability of Co causing a high price, toxicity, problems with thermal stability of $LiCoO_2$ has compelled researchers to explore new cathode materials, especially for large scale applications such as hybrid and electrical vehicles and load levelling.

The person behind introducing $LiCoO_2$ as lithium ion battery cathode, Goodenough, holds not only the patent widely known as "$LiCoO_2$ patent" [41] but also the patent covering electrode intercalation process [42] while Whittingham who studied dichalcogenides holds the patent for chalcogenide battery [20].

2.5.1.3 Lithium Nickel Oxide, $LiNiO_2$

Stoichiometric lithium nickel oxide, $LiNiO_2$, is considered to have a rock salt crystal structure (α-$NaFeO_2$ structure). It is also iso-structural with lithium cobalt oxide, $LiCoO_2$. This material mainly exists as $Li_{1-x}Ni_{1+x}O_2$ due to the Ni disorder where Ni ions occupy Li sites (commonly described as the presence of transition-metal in the lithium layer in layered compounds) and the instability of Ni^{3+} ions [9,43]. The Ni disorder causes a lithium deficiency. This introduces an electro neutrality imbalance in the structure. Hence, some of the Ni should be reduced to Ni^{2+} to maintain the electro neutrality., Which means that Ni^{2+} is always present in the structure. As a result of these anomalies,

synthesising stoichiometric $LiNiO_2$ is not possible according to most reports. Loosing Li from the structure during high temperature heat treatment make the synthesis of stoichiometric $LiNiO_2$ even more difficult [43]. Consequently, it has not been studied as a lithium intercalation material in its pure form, even though Ni is cheaper and more abundant than Co. The Ni disorder reduces the mobility of the Li ions, and hence the capacity and rate capability as a lithium ion battery cathode is reduced. It has also been reported that the stability of $LiNiO_2$ is low due to the high equilibrium partial pressure of oxygen, which is caused by the low lithium content [9]. As a result, it is too dangerous to use in a commercial cell because of the risk of explosion and fire upon contact with the electrolyte solvents.

2.5.1.4 Lithium Manganese Dioxide, $LiMnO_2$

$LiMnO_2$ has been an interesting material for lithium ion battery cathode due to promising characteristics such as low cost, wide availability and environmentally friendliness. Manganese oxides are also known for being readily lithium intercalated [44]. $LiMnO_2$ is thermodynamically unstable at elevated temperatures, and cannot be synthesised by usual techniques used for synthesising for instance $NaMnO_2$ [45]. Chen *et al* [45] have introduced hydrothermal assisted lithium permanganate decomposition to synthesize $LiMnO_2$. However, in this case the result is a hydrated form of the compound, $Li_xMnO_2.nH_2O$. It is structurally similar to $Li_xTiS_2.nH_2O$ [45]. The water is removed by heating and results in dry Li_xMnO_2. Excessive heating would result in the spinel $LiMn_2O_4$, according to Chen *et al* [45].

Efforts have been made to stabilize the layered $LiMnO_2$ in order to utilize its full potential as a lithium ion battery cathode material. It is mainly done by making structural and electronic properties similar to that of $LiCoO_2$. Substitution of Mn by more electron rich Ni, Co, and double substitution of Mn by Ni and Co have successfully been attempted to achieve this goal [4,9,46-51]. Initial studies on Ni substitution, $Li_xNi_{1-y}Mn_yO_2$ for $0 < y \leq 0.5$, was not promising due to low capacity and poor rate capabilities [50]. Despite the

initial findings, Spahr *et al* [51] reported materials with Ni:Mn composition ratio of 1:1 which delivered high specific capacity and good cycle performance.

2.5.1.5 Mixed Nickel-Manganese-Cobalt Dioxide, $Li(Ni_{1-y-z}Mn_yCo_z)O_2$

Since the wake of the new millennium, layer structured $LiNi_{1-y-z}Mn_yCo_zO_2$ compounds (NMC compounds) have extensively been investigated. They are found to possess properties that qualify them as possible candidates to substitute $LiCoO_2$ [30,46,52-54]. Liu *et al* [55] and Yoshio *et al* [56] have published the first work on NMC compounds. Moreover, they also found that the nickel disorder, described in section 2.5.1.3, was reduced from 7.2% to 2.4% when Co was doped in $LiMn_{0.2}Ni_{0.8}O_2$ to form $LiNi_{0.5}Mn_{0.2}Co_{0.3}O_2$. This also leads to capacity and reversibility improvements. The symmetric compound $Li(Ni_{1/3}Mn_{1/3}Co_{1/3})O_2$ allows reversible lithium extraction up to 2/3 in contrast to 1/2 for $LiCoO_2$. Hence, the former shows a higher capacity and reversibility in addition to a higher thermal stability compared to the latter. However, the redox couple taking part in electrochemical reaction upon reversible lithium intercalation is $Ni^{2+/4+}$ in $Li(Ni_{1/3}Mn_{1/3}Co_{1/3})O_2$. A capacity of 150 mAh g^{-1} has been reported for $Li(Ni_{1/3}Mn_{1/3}Co_{1/3})O_2$ for a voltage window of 2.5 - 4.2 V, and upon increasing the upper voltage to 5 V, the capacity increases to 220 mAh g^{-1} [57]. The capacity increase indicates that the $Co^{3+/2+}$ couple also take part in the lithium de/intercalation. However, they also observed a rapid capacity fading. A capacity of 180 mAh g^{-1} has been reported over 50 cycles for the voltage window 3.0 - 4.5 V with high degree of reversibility [4]. Extensions of these NMC compounds, especially the symmetric compound $Li(Ni_{1/3}Mn_{1/3}Co_{1/3})O_2$, by further reducing the Co content has drawn much attention. These types of substituted NMC compounds are discussed further in paper III.

2.5.1.6 Spinels

The first successful effort on reversible Li^+ intercalation on a spinel material, $LiMn_2O_4$, was carried out under the guidance of Goodenough during early 1980ies. The Spinel $Li_xMn_2O_4$ shows two plateaus in its Voltage profile versus Li^+/Li for $0 \leq x \leq 2$ upon Li

removal/insertion as depicted by Figure 2.3, adopted from Ref.6. However, during the 1980ies, researchers focused mainly on the lithium ion battery cathode materials in the charged state. This concept was decisively changed when the SONY introduced a lithium ion battery with the cathode in the discharged state. $LiMn_2O_4$ was one of the first materials to be investigated as cathode assembled in the discharged state.

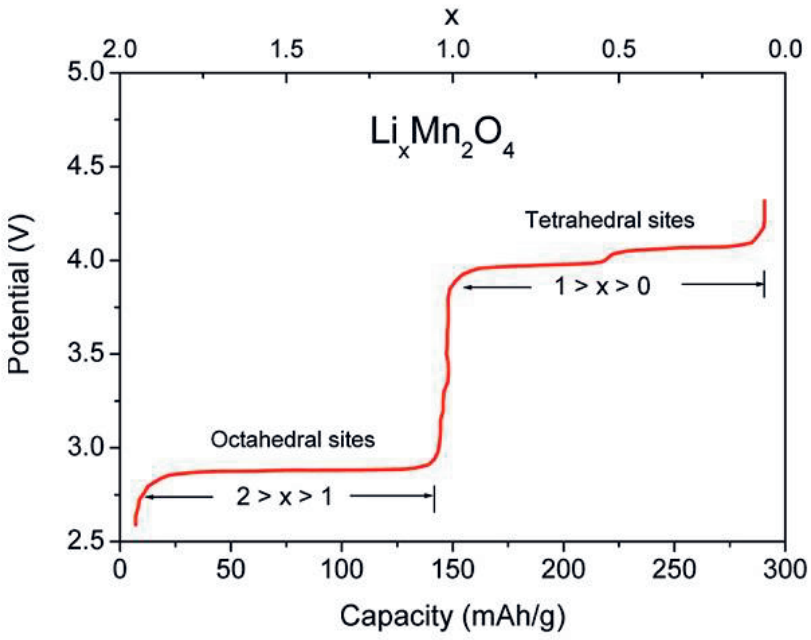

Figure 2.3 *Potential vs. Li^+/Li profile of spinel $Li_xMn_2O_4$ for complete reversible lithium intercalation ($0 \leq x \leq 2$) [6].*

Goodenough and Kim [6] described that Li^+ would be inserted into the 16c octahedral sites in the $LiMn_2O_4$ spinel structure. In this position, it would share two faces with the cations at the tetrahedral 8a sites, Figure 2.4, adopted from Ref. 6.

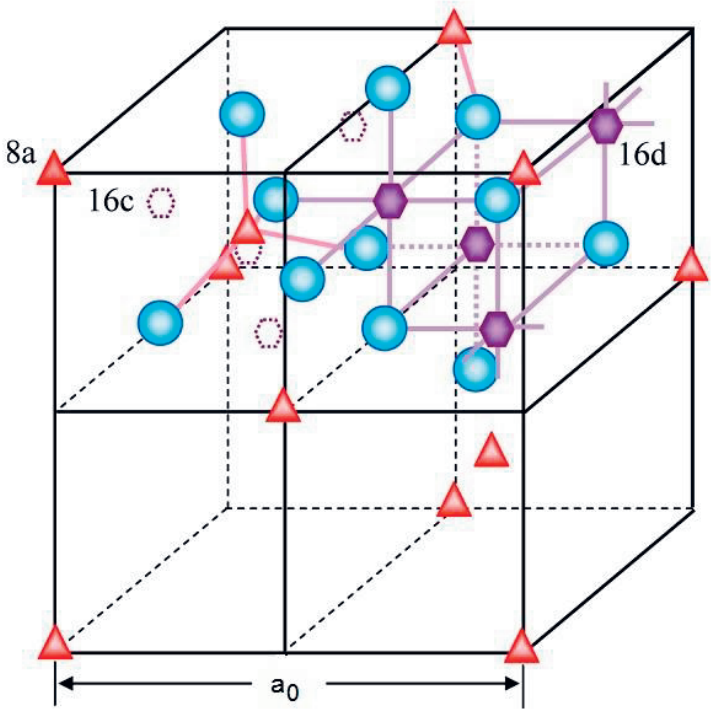

Figure 2.4 *Unit cell structure of cubic spinel which depicts the site occupation; occupied sites (8a and 16d), unoccupied sites (16c) [6].*

The $LiMn_2O_4$ cathode, however, suffered an irreversible capacity loss in the 4 V plateau range. Researchers have tried to overcome this by substituting Mn with other cations such as Mg, Cr, Fe and Cu [58-61]; and coating $LiMn_2O_4$ particles with, for example ZnO, Al_2O_3 [62,63]. Among the studied substituted $LiMn_2O_4$ materials, $LiNi_{0.5}Mn_{1.5}O_4$ soon gained much attention as another promising class of cathode materials. A detailed description on reversible lithium intercalation in spinel materials and a discussion on $LiNi_{0.5}Mn_{1.5}O_4$ are presented in the introduction of papers I and II.

2.5.2 Lithium Iron Phosphate, $LiFePO_4$

Towards the end of last millennium another class of lithium ion battery cathode materials with the composition Li*M*PO_4 (*M* = Fe, Mn, Co, Ni) was introduced under the

guidance of Goodenough [64]. These materials were called phospho-olivines because of the structural similarity with the mineral olivine, $(Mg,Fe)_2SiO_4$. Anderson *et al* [65] and Yang *et al* [66] soon reported $LiFePO_4$ to be the most promising candidate for a lithium ion battery cathode amongst these materials. $LiFePO_4$ is environmentally benign, cheaper, and thermally stable compared to $LiCoO_2$. The material has an attractive voltage of 3.45 V *vs.* Li/Li^+, which is easy to work with and a high theoretical capacity of 170 mAh g^{-1}. Moreover, these features are essentials in order for a material to be competing with $LiCoO_2$. However, for a long time the commercial introduction of $LiFePO_4$ was hindered by one major drawback; its poor electronic conductivity. Several pathways were explored to overcome this problem. Ravet *et al* [67], Huang *et al* [68], and Dominko *et al* [69] tried to coat the $LiFePO_4$ particles with a conductive carbon layer. Yamada *et al* [70], Yang *et al* [71], and Prosini *et al* [72] attempted decreasing the actual size of the $LiFePO_4$ particles, and cycling the batteries with $LiFePO_4$ cathodes at a higher temperature than room temperature. However, all these attempts only partially solve the problem of low electronic conductivity. Attempts to increase the electronic conductivity by doping the $LiFePO_4$ have also been made. When all these methods are combined, the practical capacity of the $LiFePO_4$ cathodes approaches its theoretical value (170 mAh g^{-1}).

Nytén *et al* [73] showed that reversible Li^+ extraction of Li_2FeSiO_4 was possible according to the reaction;

$$Li_2FeSiO_4 \leftrightarrow LiFeSiO_4 + Li^+ + e-$$

This gives a theoretical capacity of 166 mAh g^{-1}, which is very close to that of $LiFePO_4$. Many of the positive attributes of $LiFePO_4$ also apply for Li_2FeSiO_4 as well. However, similar to $LiFePO_4$, there is also a problem with low electronic conductivity for Li_2FeSiO_4. Moreover, by using the same approaches as for $LiFePO_4$ it would be possible to go a long way towards full utilisation of Li_2FeSiO_4 as a cathode material.

2.6 Anode materials for the lithium ion battery

Graphite or carbon-based materials are among the most attractive anode materials used in today's commercial lithium-ion batteries [3,6,74]. The main reasons for this are good cycling performance of carbonaceous materials and the low cost. Graphite can accommodate up to one lithium atom per six carbon atoms by forming the compound LiC_6. it has a gravimetric capacity of 372 mAh g^{-1} [75]. There is also a group of anode materials which have recently been investigated extensively, but have not yet reached commercialization. These are the lithium metal alloys, Li_xM, where *M* is typically Al, Sn, Si or Sb [3,75,76]. These materials generally give very high volumetric capacities. One main problem, however, is the high volume expansion and contraction during cycling related to their ability to accommodate large amounts of lithium atoms. This results in structural degradation and severe reduction of cycle life. One solution to this problem is the use of inter-metallic compounds such as AlSb, Cu_6Sn_5 and Cu_2Sb [77-79]. The volume changes in these compounds are much smaller compared to the lithium metal alloys. The reason for this is that these inter-metallic compounds contain a second element, which is usually not electrochemically active (Al in AlSb and, Cu in Cu_6Sn_5 and Cu_2Sb) but can buffer the volume expansion and contraction during cycling.

Another set of potential materials that can be used as anode materials, though of little interest, is lithium transition metal oxides having rock salt structure [2,3,6,9,78,80].

Even though much work is done on the anode materials, graphite still dominates as the preferred anode for commercial lithium ion batteries. The anode materials will not be discussed further, as the focus of this thesis is lithium ion battery cathode materials.

2.7 Electrolytes

Electrolytes represent the third key component of an electrochemical cell. The choice of electrolyte is crucial, though, its role is usually considered trivial. The selection criteria of the electrolyte differ depending on whether it is for polymer or liquid-based lithium ion rechargeable batteries [5,6,81]. For a highly oxidizing (> 4V versus Li/Li^+) lithium ion battery cathode material, such as $LiNi_{0.5}Mn_{1.5}O_4$ spinel, electrolyte combinations that operate well outside their window of thermodynamic stability (3.5 V) are required. This was one of the reasons why early lithium ion battery researchers ignored cathode materials having a higher potential.

When considering an electrolyte for a battery system, the electrolyte must meet several other conditions in addition to a large electrolyte window (E_g). Those conditions can be summarized as follows [6];

(1) Retention of the electrode/electrolyte interface during cycling when the electrode particles are changing their volume.
(2) A Li^+ ion conductivity $\sigma_{Li} > 10^{-4}$ S/cm over the temperature range of battery operation.
(3) An electronic conductivity $\sigma_e < 10^{-10}$ S/cm.
(4) A transference number $\sigma_{Li}/\sigma_{total} \approx 1$, where σ_{total} includes conductivities by other ions in the electrolyte as well as $\sigma_{Li} + \sigma_e$.
(5) Chemical stability over ambient temperature ranges and temperatures in the battery under high power.
(6) Chemical stability with respect to the electrodes, including the ability to form a passivating solid/electrolyte-interface (SEI) layer rapidly, where kinetic stability is required because the electrode potential lies outside the electrolyte window.
(7) Safe materials, i.e., preferably non-flammable and non-explosive if short-circuited.
(8) Low toxicity and low cost.

Nevertheless, achieving all these conditions has been a challenging task up to date. Figure 2.6, adopted from Ref. 6, gives a comparison of the voltage versus capacity of several electrode materials relative to the window of the electrolyte 1 M $LiPF_6$ in EC/DEC (1:1).

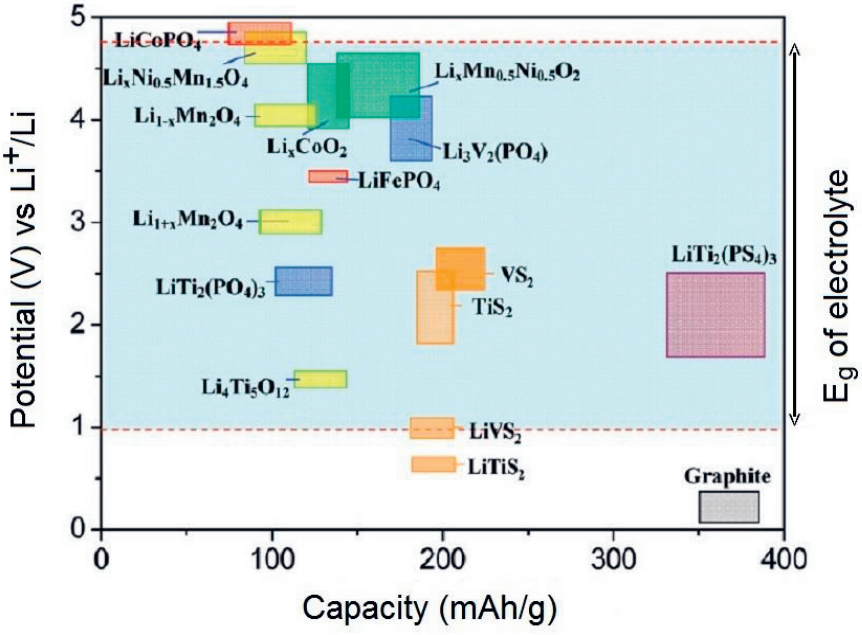

Figure 2.5 *Comparison of electrochemical stability of several lithium ion battery cathode materials relative to the electrochemical window of the electrolyte, 1 M $LiPF_6$ in EC/DEC (1:1) [6].*

Mixtures of ethylenecarbonate, diethylcarbonate and dimethylcarbonate as solvent and hexafluorophosphate ($LiPF_6$) as salt are used in most commercial electrolytes [82]. However, the search of new electrolytes with higher thermal stability and stability at higher potentials is of great importance and is an ongoing task.

An electrolyte solution containing 1 M $LiPF_6$ in a 1:1 (weight ratio) ethylene carbonate:dimethyl carbonate (EC:DMC) was used in the electrochemical testing of the materials reported in the present work.

2.8 Nanomaterials

Nanostructured materials are currently of interest for lithium ion battery electrode materials because of their high surface area and porosity. According to Aifantis and Dempsey [83] these characteristics make it possible to introduce new active reactions, decrease the Li^+ diffusion length, reduce the specific surface current rate, and improve stability and specific capacity. Moreover, composite nanostructured materials designed to include electronic conductive paths could decrease the inner resistance of lithium ion batteries, leading to higher specific capacities even at high charge/discharge current rates. Nanomaterials have widely been applied in many fields. During the last ten years, researchers have tried to incorporate nanostructured materials in energy storage devices as well [84,85]. Lithium ion battery researchers are in the process of utilizing these nanostructured materials as electrodes in order to achieve high charge/discharge current rates [86]. It is usually desirable that the amount of energy stored in a given mass or volume of the lithium ion battery is as high as possible. The development of nanostructured electrodes is considered the most promising route to achieve this aim. Moreover, the potential advantages of nanostructured active electrode materials can be summarized as follows,

a) Most of the lithium sites can be accessed using nanomaterials. This is not always possible with bulk materials, for example $LiFePO_4$.
b) Nanomaterials provide a larger electrode/electrolyte contact area, which leads to higher charge/discharge rates.
c) Nanomaterials lead to short path lengths for both electronic and Li ion transport. This allows operation at high rates (high power) though the electronic or Li ion conductivity of a material is low.

3. MATERIAL SYNTHESIS

3.1 Introduction

Synthesis of ceramic powder is a crucial factor in the field of electro-ceramics. The powder characteristics can affect the subsequent processing steps and influence the properties of the final product. Powder characteristics depend mainly on the synthesis route and synthesis conditions.

3.2 Methods used for synthesizing lithium ion battery electrode materials

There are many methods used to synthesize ceramic oxide powders. Some common methods used for synthesizing lithium ion battery electrode materials, which are mainly ceramic oxides, are hydrothermal preparation, mix hydroxide method, sol-gel method, glycine-nitrate method and Pechini method. These methods are relatively inexpensive and do not require sophisticated equipment. In addition, such techniques as Atomic Layer Deposition (ALD), Chemical Vapour Deposition (CVD) and Physical Vapour Deposition (PVD) can be used to modify and improve the properties of the powder materials. Nevertheless, such methods are expensive and need technically advanced equipment, and hence increase the cost of production significantly.

3.2.1 Hydrothermal Method

Hydrothermal approaches utilize pressure as a means to heat water to temperatures above its normal boiling point in order to increase the reaction rate between solids. The reactants should be partly soluble in water at higher temperatures, which allows intimate mixture and rapid reactions into a more stable product. Under these conditions, reactions may occur at much lower temperatures than in the absence of water, i.e. solid state synthesis [87].

Possible advantages of the hydrothermal method over other types of crystal growth include the ability to create crystalline phases that are not stable at the melting point and avoid loss of volatile elements during synthesis. The method is also particularly suitable for growth of large good-quality crystals while maintaining good control over their composition. Disadvantages of the method include the need of expensive autoclaves and not being able to follow the reaction as it proceeds.

Huang *et al* [88] have used this method to synthesise nano sized Li $Ni_{0.5}Mn_{1.5}O_4$ spinel materials. They have reported a capacity of 100 mAh g^{-1} for a voltage window of 2.0 - 4.95 V.

Despite the good reaction conditions, the overall performance of materials synthesised by the hydrothermal method is low compared to the other synthesis methods such as sol-gel and glycine-nitrate method, as will be mentioned bellow.

3.2.2 Mixed Hydroxide Method

The mixed hydroxide method is a co-precipitation method where the metal cations are precipitated as hydroxides. This is then followed by a heat treatment at high temperatures. Synthesis of $Li(Ni_{1/3}Mn_{1/3}Co_{1/3})O_2$ by mixed hydroxide method is described below as an example [89].

An aqueous solution of the metal nitrates is made with a cation ratio, Ni:Mn:Co = 1:1:1. The precipitation of $M(OH)_2$ (M = Ni, Mn, Co) is achieved by slowly dripping the nitrate solution from a burette to a solution of 1 M LiOH with continuous stirring. The filtrated precipitate is washed with de-ionized water twice to remove the residual Li salt. The product is then dried in air at 180 °C for 12 h, mixed with stoichiometric amount of $LiOH{\cdot}H_2O$ and finally ground in an auto grinder before the powder is pressed into pellets. The pellets are initially heated to 480 °C for 4 h for impregnation of the LiOH into the

matrix. The product is cooled, reground and pelletized before heated at 1000 °C for 12 h, followed by quenching to room temperature.

$Li(Ni_{1/3}Mn_{1/3}\ Co_{1/3})O_2$ which was prepared as described above, achieved a capacity of 143 mAh g^{-1} for 2.5 - 4.4 voltage range which was stable for 40 cycles.

3.2.3 Sol-gel process

The sol-gel process is a wet-chemical technique (Chemical Solution Deposition) for the fabrication of materials (typically a metal oxide) starting either from a chemical solution ("sol" short for solution) or colloidal particles ("sol" for nanoscale particle) to produce an integrated network (gel). Typical precursors are metal alkoxides, for example metal acetates, which undergo hydrolysis and polycondensation reactions to form a colloid, a system composed of solid particles (size ranging from 1 nm to 1 µm) dispersed in a solvent. The sol evolves then towards formation of an inorganic continuous network containing a liquid phase (*gel*). Formation of a metal oxide involves connecting the metal centers with oxo (*M*-O-*M*) or hydroxo (*M*-OH-*M*) bridges, therefore, generating metal-oxo or metal-hydroxo polymers in solution. The drying process serves to remove the liquid phase from the gel thus forming a porous material. Then a thermal treatment (firing) may be performed in order to favour further polycondensation and enhance mechanical properties.

The precursor sol can be either deposited on a substrate to form a film (e.g. by dip-coating or spin-coating), cast into a suitable container with the desired shape (e.g. to obtain a monolithic ceramic, glasses, fibres, membranes, aerogels), or used to synthesize powders (e.g. microspheres, nanospheres). The sol-gel approach is interesting in that it is a low cost and low-temperature technique that allows for the fine control on the product's chemical composition. Even small quantities of dopants, for example rare earth metals, can be introduced in the sol and end up in the final product finely dispersed. It can be used in ceramic manufacturing processes, as an investment casting

material, or as a means of producing very thin films of metal oxides for various purposes. Sol-gel derived materials have diverse applications in optics, electronics, energy, space, (bio)sensors, medicine (e.g. controlled drug release) and separation (e.g. chromatography) technology.

The interest in sol-gel processing can be traced back to the mid-1880s with the observation that the hydrolysis of tetraethyl orthosilicate (TEOS) under acidic conditions led to the formation of SiO_2 in the form of fibres and monoliths. Sol-gel research has grown to be so important that in the 1990ies more than 35,000 papers were published worldwide on the process [90,91]. However, the sol-gel process needs a longer calcination time compared to other liquid mix methods such as the Glycine-Nitrate method and Pechini method [92].

Ein-Eli *et al* [61] have reported that they prepared the $LiMn_{2-x}Cu_xO_4$ ($0 \leq x \leq 0.5$) spinel compositions by sol-gel process and thereby achieved nearly phase pure spinel for the composition $LiMn_{1.5}Cu_{0.5}O_4$. They achieved a capacity of 112 mAh g^{-1} for x = 0.1 and voltage window 3.3 - 4.5 V. Sun *et al* [62] reported to achieve an initial capacity close to 125 mAh g^{-1} for $LiMn_2O_4$ spinel prepared using sol-gel technique for 3.4 - 4.3 V range.

3.2.4 Glycine-Nitrate Process

The glycine nitrate method is a rapid and self-sustaining combustion process that is particularly useful for synthesising very fine, multi-component oxide powders [93]. In this method the nitrate compounds, glycine, and water are stirred and slowly heated on a hotplate. Suddenly at around 180 °C, the paste auto-ignites at around 1450 °C and blasts ceramic powders into the atmosphere. The nano scale powder is then collected and sintered into compatible ceramics. Because this scorching reaction occurs so fast, the powder is ultra-fine and chemically uniform, and thus, the ceramic have typically better properties.

Zhu and Akiyama [94] have recently used this technique for synthesizing a Li $Ni_{0.5}Mn_{1.5}O_4$ spinel material, and claim to have achieved phase pure materials. They measured a capacity of ca 125 mAh g^{-1} for a voltage window of 3.3 - 4.9 V.

3.2.5 Pechini Method

The Pechini method [95], which proceeds via an intermediate resin, is based on the ability of certain alpha hydroxyl carboxylic acids to form polybasic acid chelates with metallic ions. The chelate undergoes poly-esterification when heated with a polyalcohol and forms a viscous resin, a glassy polymer and finally a fine oxide powder upon further heating [95]. The process flow chart of the Pechini technique is shown in Figure 3.1.

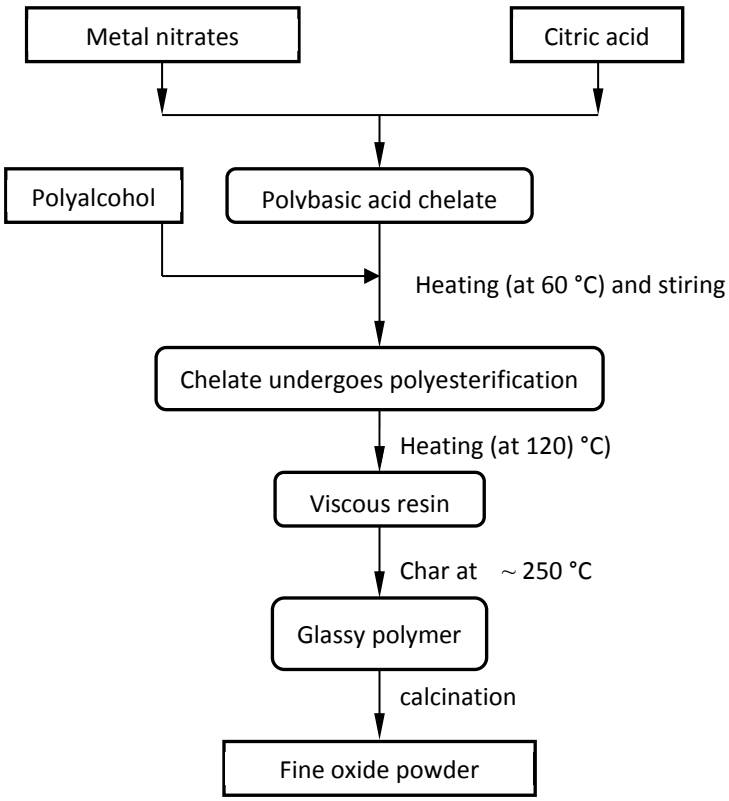

Figure 3.1 *The process flow chart of the Pechini technique.*

This technique has been used for successful synthesis of $Li(Ni_{1/3}Mn_{1/3}Co_{1/3})O_2$. The material reached a stable capacity of 180 mAh g^{-1} over 50 cycles for a range of 3.0 - 4.5 V [4]. It is also used in the present work for synthesizing spinel phases and substituted NMC compositions.

Following chapter presents an introduction to the scope of the present work.

4. THE PRESENT WORK

The ongoing performance improvement of lithium ion battery technology is mainly based on the development of materials for the various battery components, especially for the cathode. Various classes of materials have been investigated as cathode materials for lithium ion batteries to replace $LiCoO_2$ since SONY introduced the first commercial lithium ion battery. However, regardless of the immense efforts devoted to develop lithium ion battery cathode materials, the present cathode materials for lithium ion batteries still suffer from limitations connected with production costs, cyclability, capacity, electronic conductivity and potential hazard for the user and environment.

Spinel $LiNi_{0.5}Mn_{1.5}O_4$ and layered NMC compounds, $LiNi_{1-y-z}Mn_yCo_zO_2$, are such promising materials as alternatives to $LiCoO_2$, as explained under the section 2.5, for the lithium ion battery cathode materials. Even though the structural and electrochemical properties of these materials have previously been studied extensively, there are still opportunities for alternative approaches and possible improvements.

The aim of the present work can be summarized as follows:

Papers I and II focus on an extensive study of the material characteristics and electrochemical behavior of the 3D spinel $LiNi_{0.5}Mn_{1.5}O_4$ material synthesized by the Pechini technique. This spinel material attracted the attention of battery researchers, due to its high cell potential vs. Li/Li^+ leading to a higher energy density, and as a promising alternative to $LiCoO_2$. However, there have been many factors affecting the performance of this material as a lithium ion battery cathode. For example, vast difference in reported structural and electrochemical properties primarily depends on adopted synthesis methods and heat treatment conditions. Furthermore, presence of a rock salt type impurity phase, $Li_xNi_{1-x}O$, results in decrease in capacity due to loss of active material. The complex nature of the material and interest are further increased by the existence in two crystallographic structures, Ni-Mn *ordered* phase ($P4_332$) and

disordered phase (*Fd*-3*m*), which results in almost identical XRD patterns. The *disordered* structure has been widely studied, most probably due to the comparatively easy synthesis routes. Moreover, the majority of the comparative studies on the electrochemical properties of the *ordered* and *disordered* $LiNi_{0.5}Mn_{1.5}O_4$ do not account for the possibility of partial Ni-Mn ordering. In such an event, Ni and Mn have a preference for, but are not exclusively sitting on their two crystallographic sites. Those studies have used X-ray diffraction (XRD,Cu$K\alpha_1$) to investigate the crystal structure, which is not a suitable tool for characterizing Ni-Mn distribution compared to neutron diffraction and synchrotron. Moreover, *in-situ* synchrotron studies can provide more details on structural and electrochemical behavior.

Paper III is a continuation of my Master's Degree work performed in Sri Lanka and Sweden. The Master's work showed that the symmetric NMC compound, $Li(Ni_{1/3}Mn_{1/3}Co_{1/3})O_2$, is capable of reversibly extract 2/3 of the lithium compared to 1/2 from $LiCoO_2$ [4]. Moreover, a preliminary electrical conductivity study on Mg, Fe and Al substituted NMC compounds, [$Li(Ni_{1/3}Mn_{1/3}Co_{1/3-x}M_x)O_2$ *M*= Mg, Fe, Al; x = 0.11, 0.22, 0.33] indicated that the electrical conductivity of those materials were higher than that of $Li(Ni_{1/3}Mn_{1/3}Co_{1/3})O_2$. In the present work, study of substituted $Li(Ni_{1/3}Mn_{1/3}Co_{1/3})O_2$ was extended to include the structural and electrochemical characteristics. This work was carried out under the guidance of my former supervisors (during my Master's Degree work) from Institute of Fundamental Studies (IFS), Kandy, Sri Lanka and Royal Institute of Technology (KTH), Stockholm, Sweden. Under this, expansion of 2D layered symmetric NMC compound, $Li(Ni_{1/3}Mn_{1/3}Co_{1/3})O_2$, by further reducing the amount of costly Co, replacing it with cheaper elements such as Fe, Al, Mg was studied. From the ionic radii of various cations [96] (given in Table 4.1), it is more likely to form a substitutional solid solution when the Co^{3+} is replaced by Fe^{3+} and Al^{3+} cations due to the closeness of their ionic radii. However, upon substitution of Mg^{2+} for Co^{3+}, a gradual change and collapse of the structure is expected due to the higher ionic radius of Mg^{2+}.

Table 4.1 Ionic radii of various cations.

Ion →		Co^{3+}	Mg^{2+}	Fe^{3+}	Al^{3+}
Radius (Å)	At coordination number 4	---	0.57	0.49	0.39
	At coordination number 6	0.55	0.72	0.55	0.54

Paper IV focuses on the reversible Li^+ insertion in to 1D rutile structured $CrNb_2O_6$ and columbite structured $FeNb_2O_6$ materials. Niobates with structures related to the TiO_2 oxides (rutile) are considered as a useful class of lithium intercalation materials. Columbite is one such structure where previous studies showed that Li^+ can be inserted into the columbite materials, MNb_2O_6 (M = Mn, Co, Ni, Cu, Zn, Cd, Ca, Mg) [paper IV]. However, columbite structured $FeNb_2O_6$ and rutile structured $CrNb_2O_6$ have not been studied as lithium intercalation materials before. The theoretical capacity for these compounds assuming a three electron transfer process to reduce the Nb^{5+} to Nb^{2+} (in total six electrons for the two Nb in each formula unit) is 476 mAh g^{-1} for $FeNb_2O_6$ and 482 mAh g^{-1} for $CrNb_2O_6$. These values are very promising for lithium ion battery cathode, if a practical capacity close to theoretical capacities could be achieved.

In addition to the presented papers, this thesis includes unpublished results obtained on spinel materials, $LiNi_{0.5-x}Mn_{1.5+x}O_4$ (x = 0.1, 0.2) spinels and Co substituted spinel phases; $LiNi_{0.5}Mn_{1.5-x}M_xO_4$, $LiNi_{0.5-x}Mn_{1.5}M_xO_4$ and $LiNi_{0.5-y}Mn_{1.5-y}M_yO_4$, ($M$ = Co, x = 0.0,0.1,0.2 and y = 0.05, 0.1). These results are presented in the coming chapters.

5. EXPERIMENTAL METHODS AND CHARACTERIZATION TECHNIQUES

In this chapter experimental methods and characterization techniques used in the present work, introduced in chapter 4, are presented.

5.1 Powder Synthesis

Wet-chemical powder preparation techniques are easy to perform and yield relatively pure fine powders with a good chemical homogeneity. The Pechini method described in section 3.2.5 is a wet-chemical powder preparation method. This method results in powders with properties highly desired for lithium ion battery cathode materials. Such properties are good chemical homogeneity, high purity, morphology of the resulted powder particles and particle size. Due to these factors, the Pechini method was chosen in this study for the preparation of spinel and NMC oxide powders.

5.1.1 Spinel materials

Powders of $LiNi_{0.5-x}Mn_{1.5+x}O_4$ (x = 0.0, 0.1, 0.2) were prepared by the Pechini method using ethylene glycol (EG) and citric acid monohydrate (CA) in a 4:1 molar ratio [paper I,II]. For preparation of powders, stoichiometric amounts of the corresponding metal nitrates, $LiNO_3$ (99.99 %, Aldrich), $Ni(NO_3)_2 \cdot 6H_2O$ (99.0 %, VWR) and $Mn(NO_3)_2 \cdot 4H_2O$ (98.5 %, Merck) were added to the EG and CA mixture together with distilled water. The mixture was stirred for 20 hours to await chelation. Thereafter, the mixture was heated to 120 °C to remove water and become converted into a viscous resin followed by formation of a glassy polymer. The mixture was thereafter charred at ~ 220 °C giving a raw ash product. $LiNi_{0.5}Mn_{1.5}O_4$, was heat treated as mentioned in the Table 5.1. $LiNi_{0.5}Mn_{1.5-x}M_xO_4$, $LiNi_{0.5-x}Mn_{1.5}M_xO_4$ and $LiNi_{0.5-y}Mn_{1.5-y}M_yO_4$, ($M$ = Co, x = 0.0, 0.1, 0.2 and y = 0.05, 0.1) were prepared by similarly using $Co(NO_3)_2 \cdot 6H_2O$ (≥ 99.0%, Aldrich) as the Co source. These Co substituted spinels were heat treated at 900 °C for 10 h followed at 700 °C for 10 h. A sample containing the $Li_xNi_{1-x}O$ impurity phase was obtained by

calcining the ash product at 900 °C for 60 hours. A sample with composition ("$Li_{0.2}Ni_{0.8}O$") relevant for the impurity phase was synthesized separately by the procedure in Ref.[97].

Table 5.1 Heat treatment of $LiNi_{0.5-x}Mn_{1.5+x}O_4$ materials.

x in $LiNi_{0.5-x}Mn_{1.5+x}O_4$	Sample name	Treated at (°C)	Time (h)
0.0	Mn15-600	600	20
0.0	Mn15-700	700	20
0.0	Mn15-800	800 followed by 700	10 each
0.0	Mn15-900	900 followed by 700	10 each
0.0	Mn15-1000	1000 followed by 700	10 each
0.0	Mn15-900_60	900	60
0.1	Mn16-600	600	20
0.1	Mn16-900	900 followed by 700	10 each
0.2	Mn17-600	600	20
0.2	Mn17-900	900 followed by 700	10 each

5.1.2 New layered compounds based on $Li(Ni_{1/3}Mn_{1/3}Co_{1/3})O_2$

For the synthesis of new compositions of $Li(Ni_{1/3}Mn_{1/3}Co_{1/3})O_2$, $Li(Ni_{1/3}Mn_{1/3}Co_{1/3-x}M_x)O_2$ (M = Fe, Al, Mg and x = 0.11, 0.22, 0.33) powders, the Pechini method was used as described for spinels under the section 5.1.1. Metal nitrates, $LiNO_3$, $Ni(NO_3)_2{\cdot}6H_2O$, $Co(NO_3)_2{\cdot}6H_2O$, $Mn(NO_3)_2{\cdot}4H_2O$, $Al(NO)_3{\cdot}9H_2O$, $Fe(NO)_3{\cdot}9H_2O$ and $Mg(NO)_2{\cdot}6H_2O$ of analytical grade (Merck, Germany) with 10 mole % excess lithium were used as starting materials. Based on an earlier work [4] reported on the material, $Li(Ni_{1/3}Mn_{1/3}Co_{1/3})O_2$, EG:CA ratio and calcination temperature were set to 4 and 900 °C, respectively. Heat treatment was done for 2 h at 900 °C followed by 1h at 800 °C [paper III].

5.1.3 Rutile and columbite structured materials

Stoichiometric amounts of Fe_2O_3 (99.995%) or a mix of Cr_2O_3 (99.9%) and Cr metal powder (99.9%) were ground with Nb_2O_5 (99.99%), all Sigma-Aldrich, in an agate mortar

and pestle. The powders were then pressed into 5 mm pellets, placed into alumina crucibles and vacuum sealed in quartz tubes with excess Fe (99.9%) or Cr metal as oxygen getters. The samples were then heated for 12 hours at 900 °C (Fe compound) and 1050 °C (Fe compound and Cr compound). The quartz tubes were then quenched into a dry ice-acetone slush before opening. The samples were reground prior to measurements [paper IV].

5.2 Powder characterization

5.2.1 X-ray diffraction

Phase analysis of calcined powder materials was carried out by powder X-ray diffractometry (XRD, Bruker D8 Advance in Bragg-Brentano geometry, Cu$K\alpha_1$ radiation, Ge(111) monochromator, LynxEye detector).

5.2.2 Neutron diffraction

Neutron diffraction (ND) is more advantageous for determining the Mn-Ni cation ordering of $LiNi_{0.5-x}Mn_{1.5+x}O_4$ spinel phases and studying the effect of Co doping in the structure, compared to XRD. Mn, Ni and Co have similar X-ray scattering strength and hence result in identical XRD profiles. But due to the distinctive coherent neutron scattering lengths of Mn, Ni and Co (b_{Mn} = -3.73 fm, b_{Ni} = 10.3 fm and b_{Co} = 2.49 fm) [98], ND possess better means to differentiate the Mn-Ni ordering of the material. Many comparative studies on the electrochemical properties of the *ordered* and *disordered* $LiNi_{0.5}Mn_{1.5}O_4$ do not account for the possibility of partial Ni-Mn ordering**,** where Ni and Mn have a preference for but are not distinctively occupying crystallographic sites. Those studies have used X-ray diffraction (XRD) for the crystal structure study [99,100], which is not a suitable tool for characterizing Ni-Mn distribution compared to ND.

Neutron powder diffraction (NPD) data were collected at 298 K with the PUS high resolution two-axis diffractometer at the JEEP II reactor, Kjeller, Norway.

Monochromatised neutrons with wavelength of 1.5560 Å were obtained from Ge (311) single crystals. Data were collected for $10^{o} \leq 2\theta \leq 129.95^{o}$ in steps of 0.05^{o} [paper I].

5.2.3 Synchrotron experiments

Synchrotron radiation emitted by electrons in particle accelerators is extremely intense and extends over a broad energy range from the infrared through the visible and ultraviolet, into the soft and hard X-ray regions of the electromagnetic spectrum. Synchrotron radiation is used to study many aspects of the structure of matter at the atomic and molecular scale. Moreover, synchrotron radiation is inherently advantageous compared to laboratory sources for several reasons such as; high brilliance, high collimation, high level of polarization, low emittance, large tunability in wavelength by monochromatization, pulsed light emission (pulse durations may be below one nanosecond in 3rd generation sources and close to picoseconds in 4th generation sources) which allows ultra-fast time-resolved studies. High resolution synchrotron powder diffraction can be used to detect crystalline impurities present in very low concentrations otherwise undetectable by laboratory X-ray sources. The superior nature of the synchrotron radiation is best suited for in-situ studies. Furthermore, an assessment of the electronic state of the transition metals can be carried out by Ni and Mn K edge X-ray Absorption Near Edge spectroscopy (XANES). Thereby, it is possible to determine the oxidation state of Ni and Mn in $LiNi_{0.5}Mn_{1.5}O_4$ spinel materials.

Detailed experimental conditions used for Synchrotron studies in this work are reported in paper II.

5.2.4 Profile fitting and Rietveld analysis

Collected XRD / neutron data were analysed with the program *Full-prof Suite* [101]. All Rietveld refinements on synchrotron data were performed using the General Structure Analysis Suite (GSAS) with the EXPGUI [102] interface and/or TOPAS academic.

5.2.5 Raman spectroscopy

Raman spectroscopy was used as aid to identify the space group for the $LiNi_{0.5}Mn_{1.5}O_4$ materials. The Raman spectra were recorded with a Jobin Yvon Horiba T64000 spectrograph working in single/micro mode with a 1800 rules/mm grating and an entrance slit width of 100 microns leading to a spectral width of 2.2 cm^{-1}. The light source was a Millennia Pro 12JS Nd:YVO_4 laser equipped with prism and neutral density filters to ensure high spectral purity and dimming of the power to ~ 2 mW at the sample. Raman light was collected via a confocal microscope using an Olympus 100x objective combined with a 100 micron pinhole. Each spectrum is an average of six exposures lasting 10 min. Fluorescence was estimated and subtracted by the use of moderate degree polynomial expressions. Under this frame, the spectral width became 2.2 [paper I].

5.2.6 Scanning electron microscopy (SEM)

Particle morphology investigation and particle size estimation was carried out by scanning electron microscopy (FEI Nova NanoSEM 650/ ZEISS ULTRA 55/ HITACHI SU8230 FE-SEM) [paper I,III,IV]. The oxide powder was mounted on to the sample holder surface using silver paste, graphite paste or double sided carbon tape. HITACHI SU8230 FE-SEM was used to examine the morphology of the cathode tapes [paper I].

5.3 Dense material (pellet) preparation and electrical characterization

A preliminary study was carried out to determine the optimum pressure for pressing pellets. For this, pressures ranging from 10 to 400 MPa were used. It was found that the pressures bellow 100 MPa resulted in soft green pellets while pressures above 100 MPa caused the green pellet to be brittle. Therefore, 100 MPa was selected as the optimum pressure for preparing green pellets from synthesized oxide powders. Green pellets of 12 mm diameter and with thickness of 10 mm were uni-axially pressed, using cold uniaxial

pressing at 100 MPa and subsequently sintered at 900 °C for 1 h to obtain dense pellets. The electrical conductivity of the dense pellets was measured by employing the four-probe method. For that both end surfaces of the cylindrical pellet were coated with gold paste (G3535, Agar Scientific Ltd., England) and heat treated in order to improve the adherence of the gold paste to the pellet surface and thereby to provide better contact with the electrodes of the sample holder. As seen in Figure 5.1, two shallow groves, each at about a millimetre from the respective end of the pellet, were carved on the cylindrical surface of the pellets using a hard metal tool. Then, two silver wires (A and B) were wrapped around the groves and these leads were used as reference probes, thus avoiding the interference of the high contact resistance usually present at the pellet–electrode interface. The pellet was then sandwiched between two platinum electrodes (C and D) of the sample holder. Thereafter, the sample holder was loaded into a horizontal tube furnace.

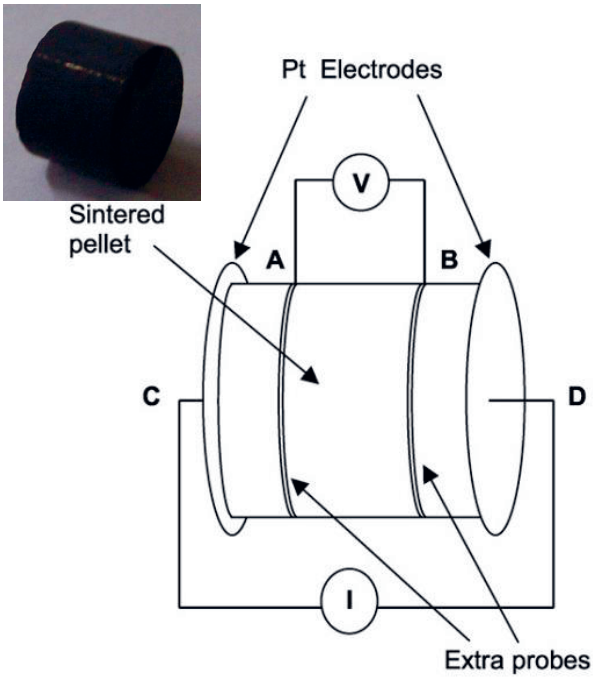

Figure 5.1 *Setup used for the four probe electrical conductivity measurement, of pellet samples[4].*

Small currents (0.1-10 mA) were applied between the terminals C and D using a dc current source (Keithly 224 programmable current source). The voltage across the leads A and B was measured using a digital multimeter (Keithly 2000). The electrical conductivity (σ) of the sample at the measured temperature was calculated using following relationship.

$$\sigma = \frac{Il}{Va} \tag{5.1}$$

where, σ is the electrical conductivity, I is the applied current, l is the distance between probes A and B, V is the measured voltage across the leads A and B, and a is the cross-sectional area of the pellet. The procedure was repeated at different temperatures from room temperature (~ 25 °C) to 150 °C, after keeping the sample at the set temperature for two hours before measuring the conductivities. For each sample, the measurements were taken while heating and cooling [paper III].

5.4 Electrode fabrication and cell assembling

An initial investigation was carried out in order to find a suitable binder for the preparation of flexible tapes using prepared oxide powders. As shown in the following Table 5.2. The combination 3 in Table 5.1 gave the best performance and hence was used for cathode preparation in this study.

Table 5.2 Various compounds used as a binder and relevant solvents used.

Binder	Solvent	Conductive additive
1.Polytetrafluoroethylene (PTFE)	NMP	super p carbon black
2. Polyvinylidenefluoride (PVDF)	Acetone/ NMP	
3.Poly(vinylidenefluoride-*co*-hexafluoropropylene) **(**PVDF-HFP)	acetone	

In order to identify the effect of cathode optimization on the specific capacity of the material, two types of composite electrodes were prepared for electrochemical testing.

A. The oxide powder was mixed with PVDF-HFP binder and Super P Carbon Black in proportions 1:0.25:0.10 by weight. The mixture was blended with acetone. After stirring, the viscous suspension was cast onto a glass plate. Thereafter, tapes for the electrodes were peeled off and dried in air for 24 hours.

B. Propylene Carbonate (PC) in a weight fraction corresponding to 40% of the active material was added to the mixture produced in A, prior to the blending with acetone. After drying, these electrodes were leached in diethyl ether (DE) to completely remove the PC.

"A" type cathodes were prepared from columbite structured $FeNb_2O_6$ and rutile structured $CrNb_2O_6$ [paper IV]. While "B" type cathodes were prepared for spinel materials and substituted NMC compositions [paper I,II,III]. The prepared electrodes had a thickness of about 100 µm.

5.4.1 Electrochemical experiments

Disks were punched out from prepared electrodes for testing in size 2032 stainless steel coin cells. The cells were assembled in an argon-filled glove box (O_2 and H_2O < 0.1 ppm). Disks of lithium metal foil were used as counter electrodes. Glass micro-fiber filters (Whatman GF/D) served as separators. The electrolyte (Merck) solution contained 1 M $LiPF_6$ in a 1:1 (weight ratio) ethylene carbonate:di-methyl carbonate (EC:DMC). A schematic cross section of the cell is given in Figure 5.2 depicting the arrangement of each part of the cell.

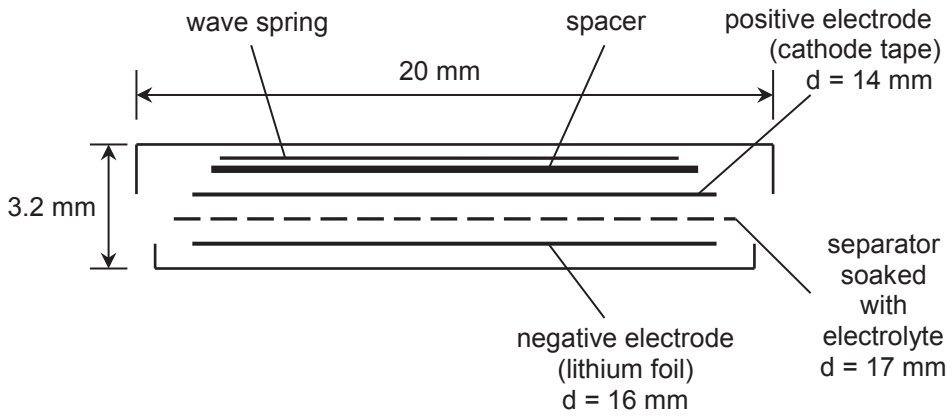

Figure 5.2 *Schematic diagram of the cross section of a 2032 coin cell.*

Galvanostatic charge-discharge experiments and cyclic voltammetry (CV) were performed using a Neware multichannel battery tester (BTS 3000) and a Biologic 16 channels MPG-2 battery tester, respectively. The cells were cycled at room temperature using following voltage windows; Spinel phases 3.0/3.5 - 4.9 V [paper I,II], substituted NMC compositions 3.0 - 4.5 V [paper III] and, $FeNb_2O_6$ and $CrNb_2O_6$ 0.5 - 3.0 V [paper IV]. For galvanostatic charge-discharge experiments, data points were collected every time when the cell voltage changed by 5 mV and/or every 5^{th} second.

6. RESULTS AND DISCUSSION

In this chapter, the major results presented in the papers I - IV, introduced in chapter 4, are summarized and discussed. In addition, some of the unpublished results obtained on the spinel materials and Co substituted spinels are also presented.

6.1 Spinel phases (3D cathode materials)

Depending on the adopted synthesis routes and heat treatment conditions, the spinel $LiNi_{0.5}Mn_{1.5}O_4$ shows different structural and electrochemical properties. In the present work, the materials were synthesized by the Pechini method and heat treated at various temperatures. Even though the XRD ($CuK\alpha_1$) study suggested that neither of the materials contained the impurity phase $Li_xNi_{1-x}O$, synchrotron based XRD (λ = 0.70135 and 0.50480 Å) revealed that only the sample Mn15-600 was phase pure. This disclosed that prior claims of impurity free materials based on XRD ($CuK\alpha_1$) may be inaccurate. Raman spectroscopic studies showed that the samples Mn15-600 and Mn15-900_60 were *disordered* and other materials were *ordered*. Neutron diffraction and synchrotron experiments further confirmed this observation. Vast majority of the literature on $LiNi_{0.5}Mn_{1.5}O_4$ suggests [see introductory sections in papers I and II] that the *disordered* phase delivers stable and higher capacity compared to *ordered* phase. In contrast to this popular conclusion, galvanostatic charge discharge experiments in the present study show that the *ordered* phase delivers superior structural and electrochemical reversibility and hence the highest capacity (137 mAh g^{-1}), Figure 6.1. *in-situ* XRD (λ = 0.50480 Å) and XANES at the Ni-K edge experiments further confirm this finding. This is a considerable achievement of the present study given that Cai *et al* [103] have reported that nearly perfect Ni-Mn ordering can be achieved after treating $LiNi_{0.5}Mn_{1.5}O_4$ for 60 h at 700 °C. Electrochemical analysis of *ordered* materials shows that the separation of the plateaus for the $Ni^{2+/3+}$ and $Ni^{3+/4+}$ redox couples is less than 20 mV (see Table 6.1 and Figure 6.2), implying a very close to the ideal Ni-Mn ordering. A split of the plateau into two separate plateaus with a separation of more than 50 mV is typically associated with

the *disordered* phase, according to Cabana *et al* [104]. Kim *et al* [105] and Lee *et al* [106] report that the separation is 30 mV and virtually undistinguishable for the *ordered* phase. Cabana *et al* [104] reported that they observed a 60 mV plateau separation for *ordered* phase and concluded that even closer to ideal Ni-Mn ordering is required for a small voltage gap. Therefore, the *ordered* materials reported in the present study are even closer to ideal Ni-Mn ordering than those previously reported in literature.

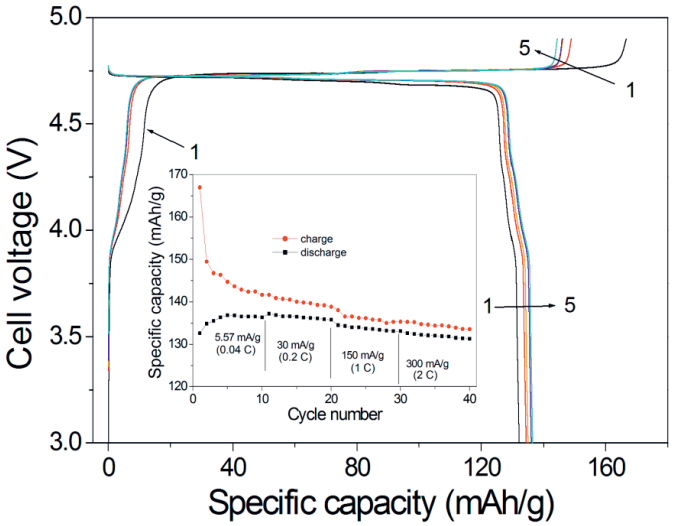

Figure 6.1 *Results of galvanostatic charge discharge experiments of sample Mn15-900, inset depicts the results of rate tests in various specific currents.*

Table 6.1 Data based on electrochemical experiments of $LiNi_{0.5}Mn_{1.5}O_4$ / Li cells (1st charge cycle).

Sample	Plateau separation at $Ni^{2+/3+}$ - $Ni^{3+/4+}$	Ordering
Mn15-600	~ 70 mV	*disordered*
Mn15-700	Not clear	*ordered*
Mn15-800	~ 20 mV	*ordered*
Mn15-900	~ 15 mV	*ordered*
Mn15-1000	Not clear	*ordered*

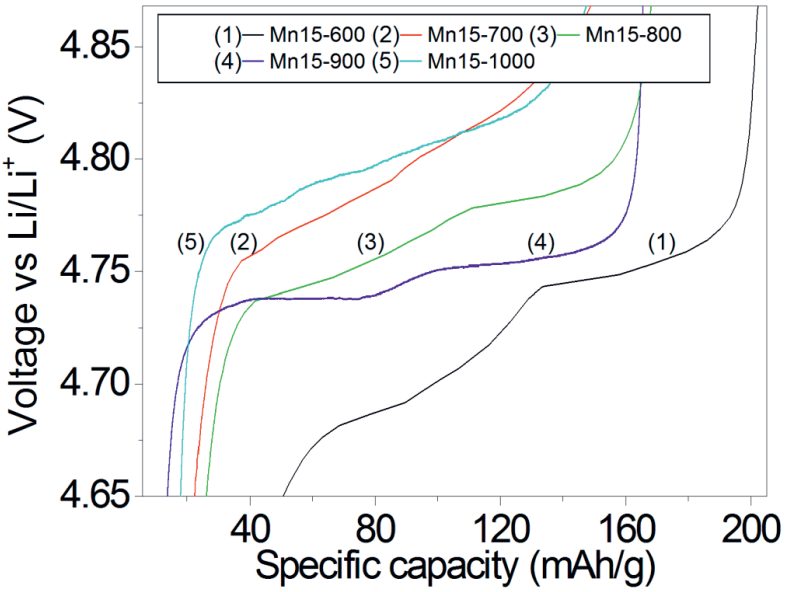

Figure 6.2 *1st charge curves of $LiNi_{0.5}Mn_{1.5}O_4$ / Li cells for 4.65-4.85V range.*

6.1.1 In-situ XRD and X-ray absorption spectroscopy

The best performing *ordered* material (Mn15-900), phase pure *disordered* material (Mn15-900) and the *disordered* material containing highest amount of rock salt impurity phase (Mn15-900_60) were selected for further *in-situ* synchrotron experiments. *in-situ* XRD (λ = 0.50480 Å) and X-ray absorption spectroscopy (XAS) analysis suggest that the *ordered* material shows two reversible phase changes, i.e. phase I to phase II and phase II to phase III in the charge-discharge cycle. The phase pure *disordered* material does not show any such phase change at all. However, the *disordered* material containing impurity shows one of these phase changes, phase I to phase II. Figures 6.3 and 6.4 illustrate these changes.

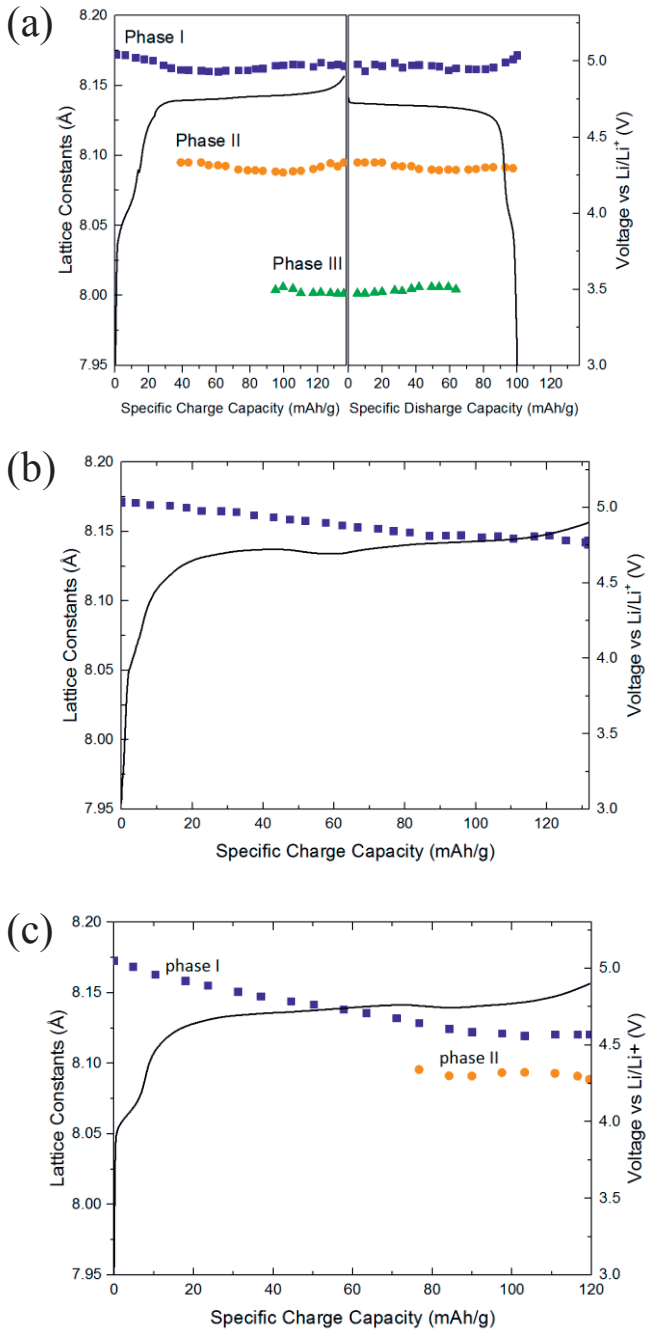

Figure 6.3 *Change of lattice constant with the capacity,* ***(a)*** *ordered material Mn15-900,* ***(b)*** *phase pure disordered material Mn15-600,* ***(c)*** *disordered material containing impurity.*

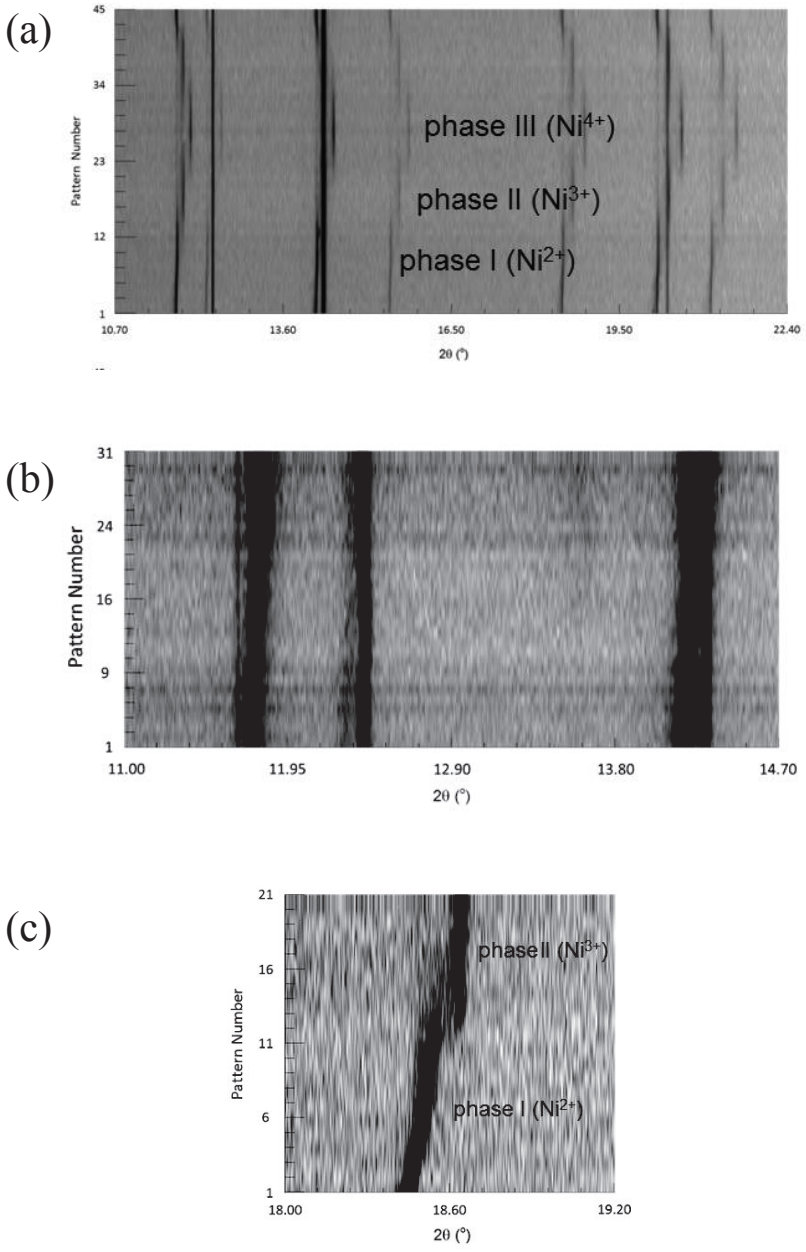

Figure 6.4 *2D projection of in-situ XRD(λ = 0.50480 Å) patterns showing phase changes* ***(a)*** *ordered material Mn15-900 showing three phases,* ***(b)*** *phase pure disordered material Mn15-600 showing single phase,* ***(c)*** *disordered material containing impurity Mn15-900_60 showing two phases.*

The two phase transitions (phase I to phase II and phase II to phase III) occur in the 4.5-4.9 V region. It is well known that in this region $Ni^{2+}/Ni^{3+}/Ni^{4+}$ oxidation/reduction takes place. Therefore, phases I, II and III can be assigned to spinel structures with Ni^{2+}, Ni^{3+} and Ni^{4+} respectively. This is confirmed by the Ni K-edge spectra of Mn15-900 sample as a function of state of discharge, Figure 6.5.

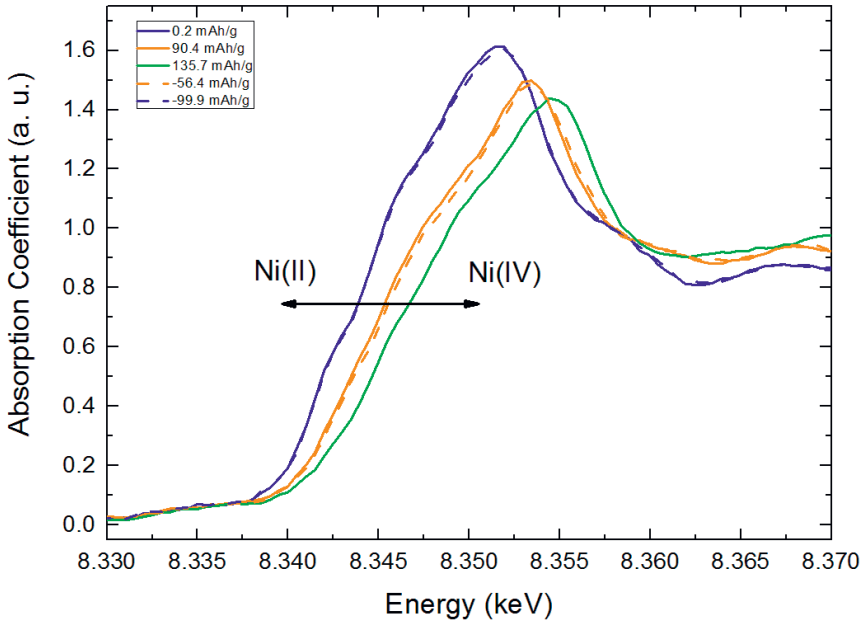

Figure 6.5 *In-situ XANE spectra (Ni K-edge) of sample Mn15-900 at maximal phase fraction showing $Ni^{2+}/Ni^{3+}/Ni^{4+}$ oxidation-recuction; solid line charge step, broken line discharge step.*

Ni K-edge spectra of the two *disordered* materials (Mn15-600 and Mn15-900_60) indicate that the Ni in those materials oxidize only up to Ni^{3+} upon charging as shown in Figure 6.6. After completing the charging step the Ni edge of these two samples are comparable to that of Ni^{3+}standard ($LaNiO_3$) within 2 eV, Figure 6.6 (b) and (f). Moreover, the Ni^{3+} to Ni^{4+} transition, which is clearly visible in the *ordered* material (see Figures 6.5 and 6.4(a)), is missing.

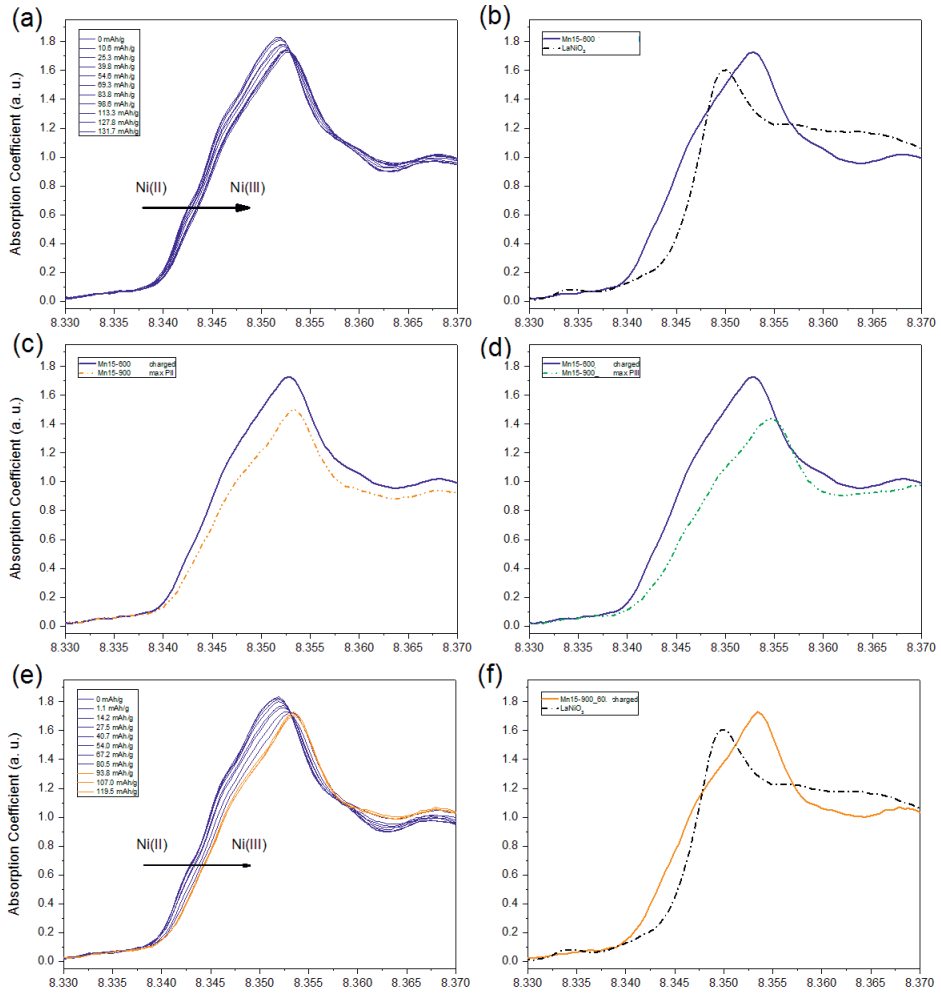

Figure 6.6 *In-situ XANE spectra (Ni K-edge) after completed first charge step;* ***(a)*** *Mn15-600 beginning to end,* ***(b)*** *Mn15-600 compared to* Ni^{3+} *standard,* $LaNiO_3$ ***(c)*** *Mn15-600 compared to maximal phase fraction of phase II of sample Mn15-900,* ***(d)*** *Mn15-600 compared to end of charge step of sample Mn15-900* ***(e)*** *Mn15-900_60 beginning to end,* ***(f)*** *Mn15-900_60 compared to* Ni^{3+} *standard,* $LaNiO_3$.

It is questionable whether all the Ni^{3+} transform to Ni^{4+} on charging for the *disordered* material. The *disordered* material may have a different redox mechanism compared to the *ordered* material. The possible option would be high valent Mn species ($Mn^{4+/5+}$)

taking part in the redox process. Unfortunately, no XANES data are available for the Mn-edge in the present study to clarify this assumption.

In summary, the present study concludes that the *ordered* phase of spinel $LiNi_{0.5}Mn_{1.5}O_4$ shows higher structural stability upon electrochemical cycling and deliver a higher specific capacity. This conclusion is supported by Raman spectroscopy, Neutron diffraction, Synchrotron experiments and electrochemical data. More details of $LiNi_{0.5-x}Mn_{1.5+x}O_4$ (x = 0.0) is reported in papers I and II.

6.1.2 Unpublished results on spinel materials

The following sections, 6.1.2.1 and 6.1.2.2, presents a discussion of the unpublished results obtained on $LiNi_{0.5-x}Mn_{1.5+x}O_4$ (x = 0.1, 0.2) spinel phases and Co substituted spinels; $LiNi_{0.5}Mn_{1.5-x}M_xO_4$, $LiNi_{0.5-x}Mn_{1.5}M_xO_4$ and $LiNi_{0.5-y}Mn_{1.5-y}M_yO_4$, ($M$ = Co, x = 0.0, 0.1, 0.2 and y = 0.05, 0.1).

6.1.2.1 $LiNi_{0.5-x}Mn_{1.5+x}O_4$ (x = 0.1, 0.2)

The study reported on $LiNi_{0.5}Mn_{1.5}O_4$ (papers I and II) showed that the highest specific capacity was obtained by the *ordered* phase of the material, produced through initial heat treatment at 900 °C. Heat treatment at 600 °C resulted in the *disordered* phase, which delivered a higher initial specific capacity but with fast capacity fading in subsequent cycling. Therefore, for further studies, 900 °C and 600 °C were selected as heat treatment conditions for the synthesis of $LiNi_{0.5-x}Mn_{1.5+x}O_4$ (x = 0.1, 0.2) spinel phases. X-ray diffraction (PXRD, $CuK\alpha_1$) profiles (see Figure 6.7) of the $LiNi_{0.5-x}Mn_{1.5+x}O_4$ (x = 0.0, 0.1, 0.2) materials in the present study suggest that all the materials are phase pure. This is an important achievement as the reported studies on spinel materials with different Mn and Ni amounts resulted in formation of the rock salt impurity phase, $Li_xNi_{1-x}O$, in their samples [58,60,61,107,108].

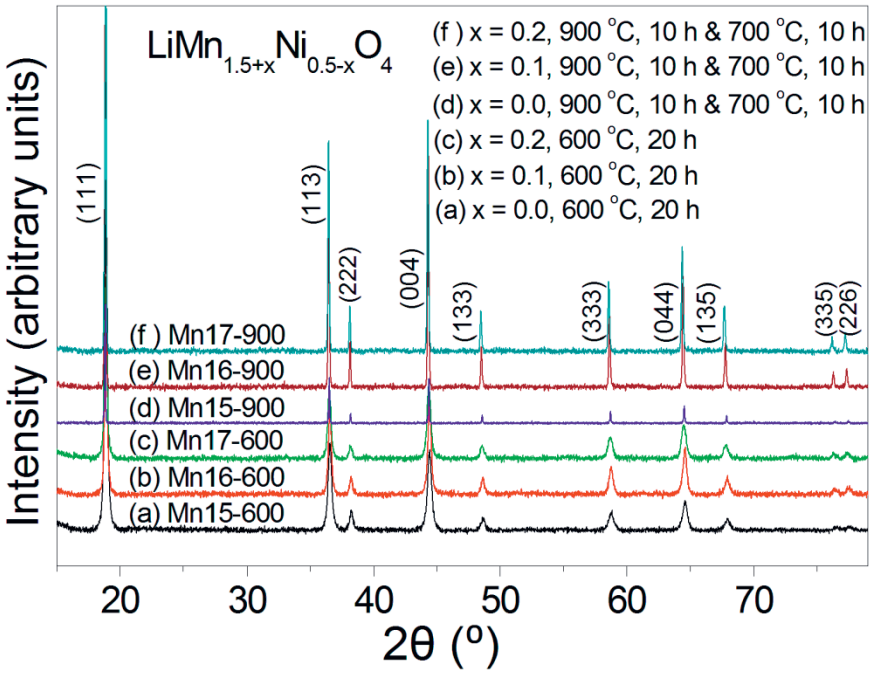

Figure 6.7 *Powder X-ray diffraction (PXRD,CuKα$_1$) profiles of the $LiNi_{0.5-x}Mn_{1.5+x}O_4$ materials. Sample information is given in the legends.*

No impurity, $Li_xNi_{1-x}O$, related Bragg peaks, which would be present close to the reflections caused by (004) and (222) planes, are visible. The reflections caused by (335) and (226) planes become more prominent with the increase of Mn content. Full width at half maximum (FWHM) of the samples treated at 600 °C are higher compared to the samples treated at 900 °C, mainly due to the nanoscale nature of the particles (See Table 6.2 for details). The sample Mn15-600 has the largest unit cell parameter (*a*) and consequently the largest unit cell volume (*V*) while Mn16-600 shows the smallest *a* and *V*. According to the powder neutron diffraction data, Mn15-600 and Mn16-600 are of *disordered* and *ordered* structure types, respectively. The *disordered* phase contain considerable amount of Mn^{3+} compared to the predominant amount of Mn^{4+} in the *ordered* phase. Having a larger ionic radius compared to Mn^{4+}, Mn^{3+} ions cause an expansion of the unit cell, resulting in larger *a* and *V* values of the *disordered* material.

Table 6.2 Structural parameters of the $LiNi_{0.5-x}Mn_{1.5+x}O_4$ powder materials based on PXRD ($CuK\alpha_1$) data.

	Sample name	FWHM at 2θ = 36.5 °	*a* (Å)	V (Å^3)	Scherrer Particle size (nm)
(a)	Mn15-600	0.289 °	8.168	544.94	36.8
(b)	Mn16-600	0.277 °	8.126	536.68	38.9
(c)	Mn17-600	0.176 °	8.139	539.15	73.1
(d)	Mn15-900	0.083 °	8.157	542.74	404
(e)	Mn16-900	0.126 °	8.153	541.87	131
(f)	Mn17-900	0.103 °	8.145	540.40	204

Powder neutron diffraction (PND) profiles of $LiNi_{0.5-x}Mn_{1.5+x}O_4$ spinel phases (x = 0.0, 0.1, 0.2), Figures 6.8.and 6.9, confirms that Mn15-600 and Mn17-900 [patterns (a) and (f)] are of the *disordered* phase while all the other samples are dominantly *ordered* with completely or partially developed super structure related reflections (patterns (b)-(e), Figures 6.8 and 6.9). Among them, Mn16-600 and Mn15-900 show the highest degree of ordering with well developed superlattice related reflections [patterns (b) and (d)]. Figure 6.9 shows the indexed superstructure related reflections. Moreover, a slight shift of the peaks towards larger d values (lower 2θ) can be observed for the Mn17-900 (pattern (f), Figures 6.8 and 6.9).

SEM pictures of the $LiNi_{0.5-x}Mn_{1.5+x}O_4$ (x = 0.1, 0.2) materials, Figure 6.10, show that the powders treated at 600 °C has a smaller particle size compared to the powders treated at 900 °C. At x = 0.1 the material consists of two distinct particle sizes at low temperature, i.e. $\sim$ 30 nm and $\sim$ 120 nm. However, at x = 0.2 low temperature treatment results in evenly distributed $\sim$ 100 nm particles. Moreover, low temperature treatment shows the signs of incomplete formation and growth of the particles while the higher temperature treatment results in well crystalline particles with clear facets.

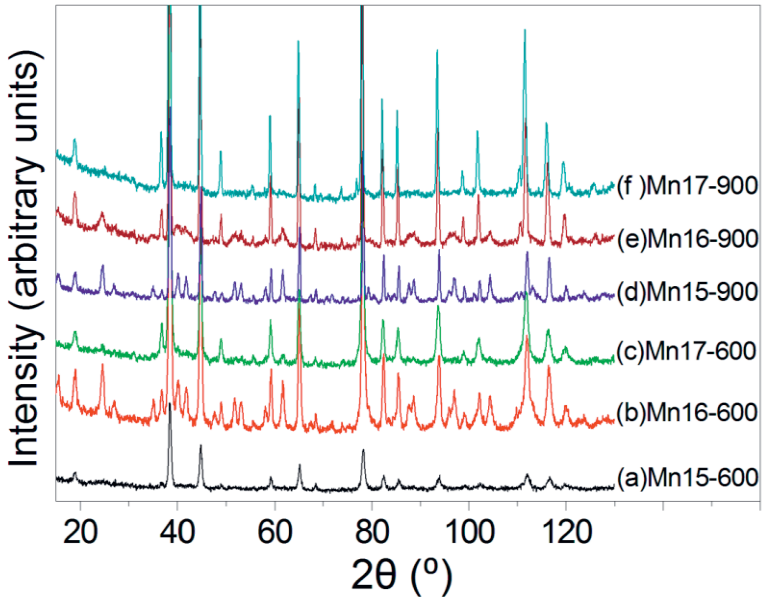

Figure 6.8 *Powder neutron diffraction profiles of the $LiNi_{0.5-x}Mn_{1.5-x}O_4$ materials.*

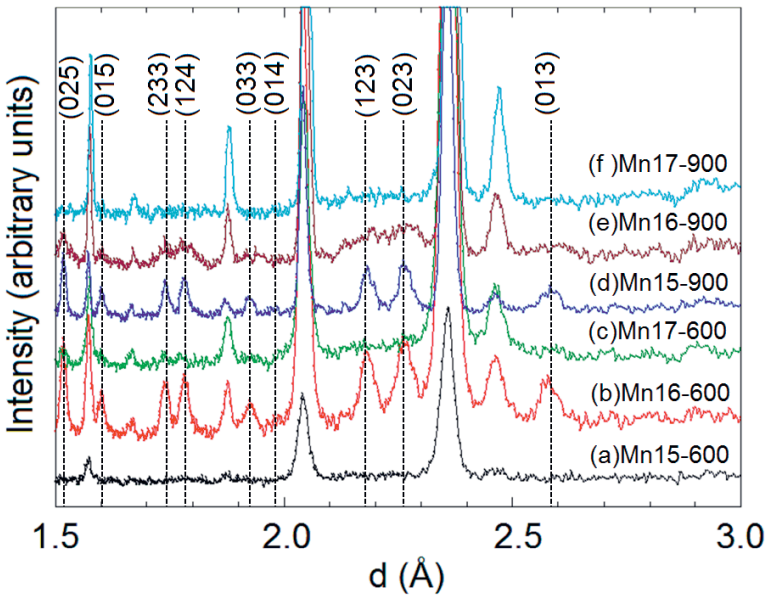

Figure 6.9 *Indexed superlattice related reflections of the $LiNi_{0.5-x}Mn_{1.5-x}O_4$ materials.*

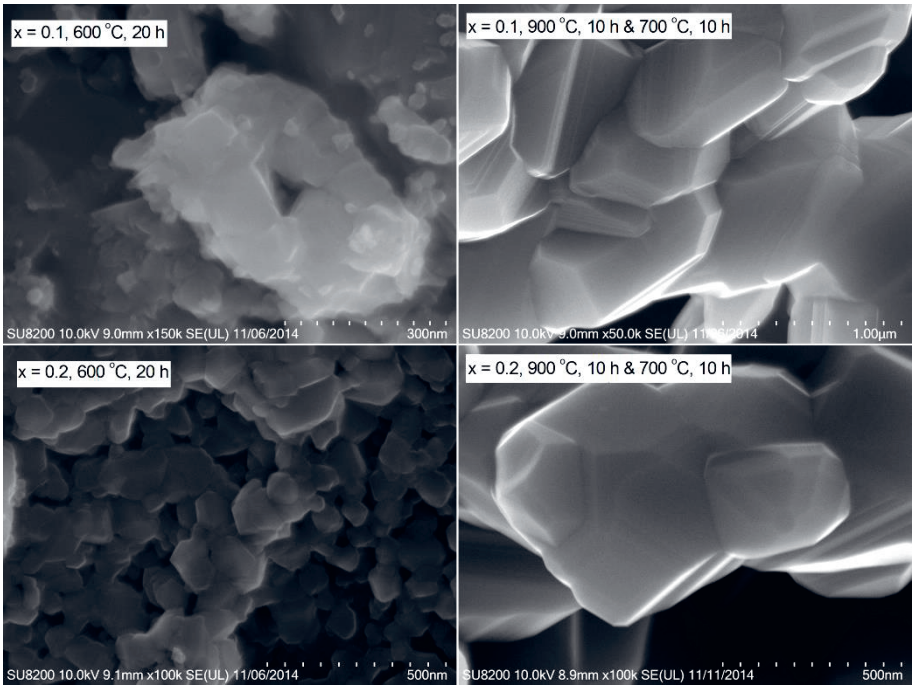

Figure 6.10 *SEM micrographs of $LiNi_{0.5-x}Mn_{1.5-x}O_4$ materials. Sample information is given in the pictures.*

Preliminary discharge capacity values obtained on these materials are shown in Table 6.3. The discharge capacity values are lower than the values reported for similar type of materials [107]. However, it is somewhat difficult to compare the values as Yi and Hu [107] do not mention at which temperature they cycled the cells. Moreover, they have used a slightly higher upper cut off voltage, 4.95 V while the present study used 4.9 V as the upper voltage limit. In addition, the discharge capacity is comparable to the values reported by Okata *et al* [109] for the above 4 V plateau. Additional analysis (not shown) also indicates that the capacity of the materials in the present study may also have been affected by remains of moisture even though they were dried. The capacity may therefore increase by improving the drying process of the cathode tapes.

Table 6.3 Discharge capacity values of the $LiNi_{0.5-x}Mn_{1.5+x}O_4$ powder materials obtained by galvanostatic experiments.

Sample	Discharge capacity (mAh g^{-1})	
	1st cycle	**10th cycle**
Mn16-600	107	95
Mn16-900	114	112
Mn17-600	92	81
Mn17-900	104	98

6.1.2.2 Co substituted spinels

Co substituted spinel phases, $LiNi_{0.5}Mn_{1.5-x}Co_xO_4$, $LiNi_{0.5-x}Mn_{1.5}Co_xO_4$ and $LiNi_{0.5-y}Mn_{1.5-y}Co_yO_4$, ($x$ = 0.1, 0.2 and y = 0.05, 0.1), were successfully synthesized using the Pechini technique. However, there is a sign of emergence of an impurity related peak in all Co substituted spinel phases, just above $2\theta = 30^o$, marked with * in Figure 6.11. The work reported by Jan *et al* [110] on these type of Co substituted spinel also show a similar bump in the same area of their XRD ($CuK\alpha_1$) patterns, though they do not discuss it. However, a more detailed study using neutron and synchrotron is required to determine if this strange peak is caused by an impurity phase or if it is caused by superlattice related reflections.

However, synchrotron studies and further electrochemical experiments could not be performed on $LiNi_{0.5-x}Mn_{1.5+x}O_4$ (x = 0.1, 0.2) and Co substituted spinels; $LiNi_{0.5}Mn_{1.5-x}M_xO_4$, $LiNi_{0.5-x}Mn_{1.5}M_xO_4$ and $LiNi_{0.5-y}Mn_{1.5-y}M_yO_4$, ($M$ = Co, x = 0.0, 0.1, 0.2 and y = 0.05, 0.1).

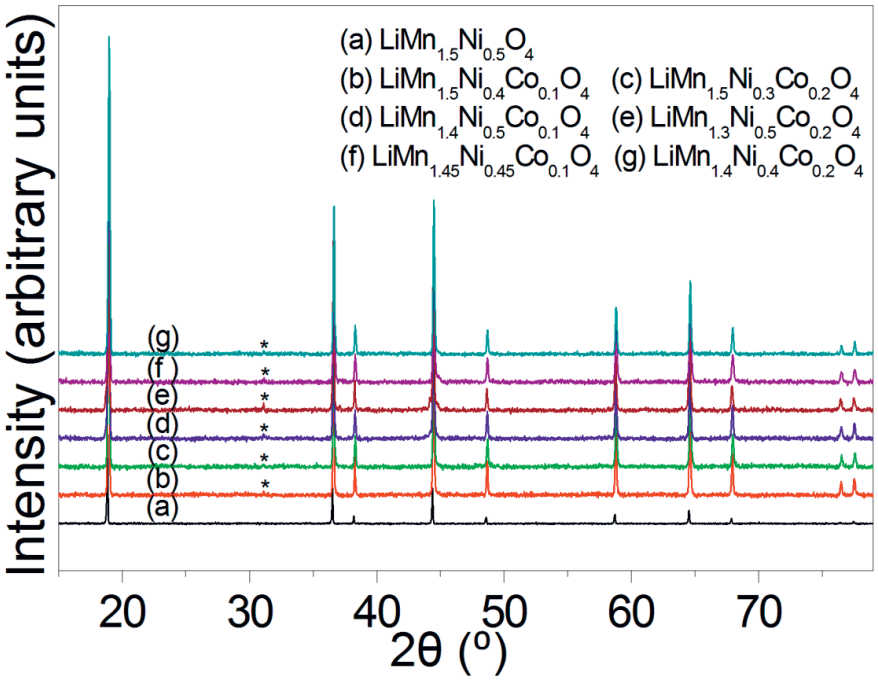

Figure 6.11 *Powder X-ray diffraction (PXRD, CuKα) profiles of Co substituted spinel phases.*

The above discussion on spinel $LiNi_{0.5-x}Mn_{1.5+x}O_4$ (x = 0.0) materials has shown that these materials synthesised by the Pechini technique possess improved structural properties and improved electrochemical behaviour. Therefore, performing detailed electrochemical and further structural studies using synchrotron on $LiNi_{0.5-x}Mn_{1.5+x}O_4$ (x = 0.1, 0.2) and Co substituted spinel materials; $LiNi_{0.5}Mn_{1.5-x}M_xO_4$, $LiNi_{0.5-x}Mn_{1.5}M_xO_4$ and $LiNi_{0.5-y}Mn_{1.5-y}M_yO_4$, ($M$ = Co, x = 0.0, 0.1, 0.2 and y = 0.05, 0.1) is important in order to explore how the variation of the Ni and Mn content affect the structure and electrochemistry. As the electrochemically active redox couple of these spinel materials is $Ni^{2+/4+}$ when the Ni content is reduced a decrease in the capacity is expected. However, it could further reduce the disorder of the materials. On the other hand, the $Mn^{3+/4+}$ and $Co^{2+/3+}$ redox couples are expected to be more electrochemically active and hence compensate the reduced capacity due to the reduction of amount of Ni.

6.2 Layered NMC compositions (2D cathode materials)

In the present work, substituted NMC materials were synthesized by the Pechini technique. After a preliminary study [4], considering factors such as preferable lower calcination temperature, lithium evaporation together with phase purity, 900 °C was selected as the optimum calcination temperature. The powder materials were heat treated at 900 °C for 2 h followed by 1h at 800 °C. PXRD ($CuK\alpha_1$) profiles obtained on layered $Li(Ni_{1/3}Mn_{1/3}Co_{1/3-x}M_x)O_2$ (M = Al, Fe, Mg and x = 0, 0.11, 0.22, 0.33) powders are shown in Figure 6.12. The phase analysis performed by X-ray diffraction on materials where Co was substituted by Al, revealed the existence of a secondary phase (marked with "+" in PXRD profiles) in all the three material compositions (0.11, 0.22 and 0.33 substitution levels) investigated in this study, Figure 6.12. The content of the secondary phase increases with the Al content of the material. In contrast, the Fe doped system shows the existence of a solid solution of the appropriate $Li(Ni_{1/3}Mn_{1/3}Co_{1/3})O_2$ phase of R-3*m* structure (α-$NaFeO_2$ layered structure) even after substituting 2/3 of Co in $Li(Ni_{1/3}Mn_{1/3}Co_{1/3})O_2$ with Fe. However, traces of a secondary phase appear in the 0.33 substitution level. Quite interestingly in the Mg added system, the original structure was retained even after replacing up to 2/3 of the Co by Mg. When all the Co is replaced with Mg, the layered structure collapsed and a new phase is formed as seen in Figure 6.13. The resulting new phase can be assigned to $Li_{0.68}Ni_{1.32}O_2$ or $Li_{0.64}Ni_{1.36}O_2$ [111], meaning the material is more related to rock salt type structure present in spinel type materials as an impurity [6,88,Paper I,II]. The reflections relevant to this new phase are marked with "#" marks in Figure 6.13.

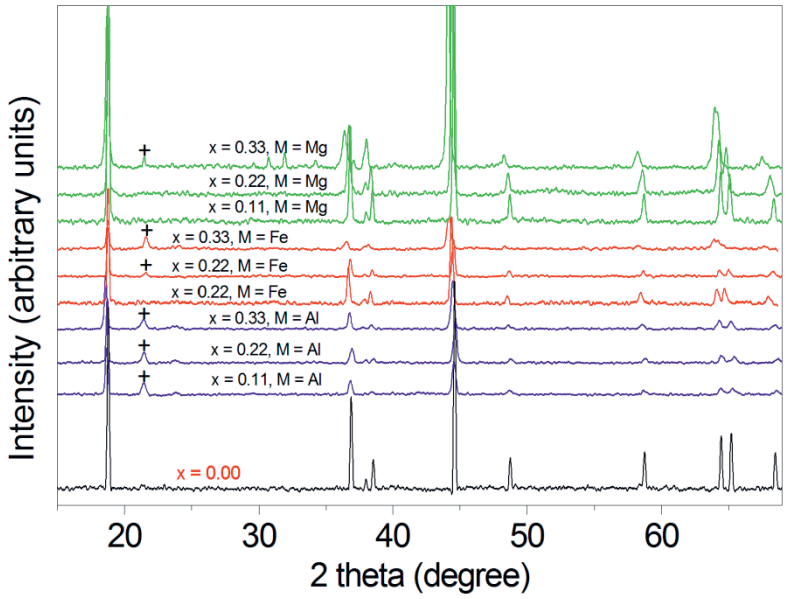

Figure 6.12 *Powder X-ray diffraction (PXRD, CuKα) profiles of substituted NMC compositions, $Li(Ni_{1/3}Mn_{1/3}Co_{1/3-x}M_x)O_2$.*

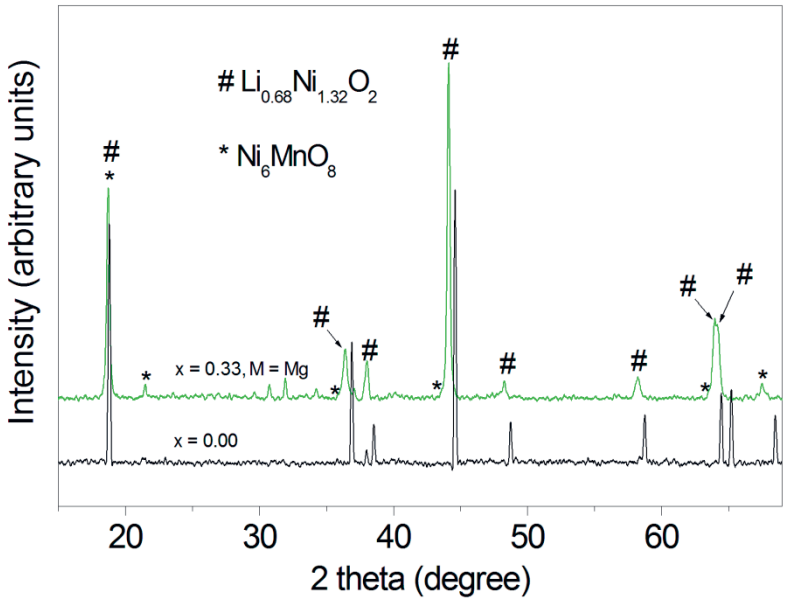

Figure 6.13 *Powder X-ray diffraction (PXRD, CuKα) profiles showing the impurity phase (*) and new phase (#) formed at the expense of layered structure.*

Hu *et al* [112] has reported that the Co doped $Li(Ni_{1/3}Mn_{1/3}Al_{1/3})O_2$ prepared via sol-gel process contain the impurity phase of γ-$LiAlO_2$. In the present study, the $Li(Ni_{1/3}Mn_{1/3}Co_{1/3-x}Al_x)O_2$ materials contain a similar secondary phase in very minute quantities for all substitutional levels as evident by the PXRD profiles. The same impurity phase that is present in the $Li(Ni_{1/3}Mn_{1/3}Co_{1/3-x}Al_x)O_2$ materials also exists in the $Li(Ni_{1/3}Mn_{1/3}Co_{1/3-x}Fe_x)O_2$ materials. Therefore, in this case, the impurity phase might not be the same as that reported by Hu *et al*. The impurity phase detected in Fe and Al substituted NMC compounds in the present study, is identified as Ni_6MnO_8 and relevant reflections are marked with "*" marks in Figure 6.13. Identifying the $Li_{0.68}Ni_{1.32}O_2$/$Li_{0.64}Ni_{1.36}O_2$ phase and detecting Ni_6MnO_8 as an impurity related to substituted NMC compositions is reported for the first time in the present work.

A study of the electrical conductivity of these types of substituted NMC compounds has not been reported before. The electrical conductivity measurements were performed by the d.c. four-probe technique, using the sintered dense pellets. The conductivity measurements were carried out from room temperature (25 °C) up to 150 °C, in static air. As expected, the electrical conductivity of all the prepared materials in the present study increases with the measuring temperature throughout the measured temperature range, indicating the semi-conducting nature of the materials. Figures 6.14-6.16 show the variation of the electrical conductivity with measured temperature of the $Li(Ni_{1/3}Mn_{1/3}Co_{1/3})O_2$ materials, where Co was substituted by Fe, Mg and Al, respectively. As shown in Figure 6.16, the substitution of Al for Co in $Li(Ni_{1/3}Mn_{1/3}Co_{1/3})O_2$, has slightly increased the conductivity up to 0.11 mole % of Al content, though the room temperature electrical conductivity is less than that of the base material, $Li(Ni_{1/3}Mn_{1/3}Co_{1/3})O_2$. Further increase of Al content has decreased the electrical conductivity and the full substitution (0.33 mole % of Al) shows a decrease of conductivity by about an order as compared to the base material. This could be resulted by the newly formed secondary phase, which increased with Al content in all those materials where Co was substituted by Al. In contrast, the conductivity increases

considerably with the Fe content to a maximum and then decreases, Figure 6.14. More interestingly, the material where 2/3 of Co was substituted by Fe (0.22 doping level) shows a considerably higher conductivity than that of the base material, $Li(Ni_{1/3}Mn_{1/3}Co_{1/3})O_2$. Again, the observed decrease in conductivity could be due to the secondary phase present in 0.33 substitutional level (i.e. Co free material). Furthermore, these materials form a solid solution of the appropriate $Li(Ni_{1/3}Mn_{1/3}Co_{1/3})O_2$ phase of R-3*m* structure up to 0.22 of Fe. It is generally interesting that an alternative cathode material where up to 2/3 of the costly Co is replaced by cheaper Fe, still possess better electrical conductivity while preserving the appropriate layered structure. Therefore, these Fe doped $Li(Ni_{1/3}Mn_{1/3}Co_{1/3})O_2$ compositions are highly potential for LIB cathode application. Moreover, electrical conductivity of Mg substituted materials is higher than that of the base material, $Li(Ni_{1/3}Mn_{1/3}Co_{1/3})O_2$, for all Mg substitution levels, Figure 6.15. The higher conductivity of Co free material can be attributed to the structural changes at x = 0.33 substitution level.

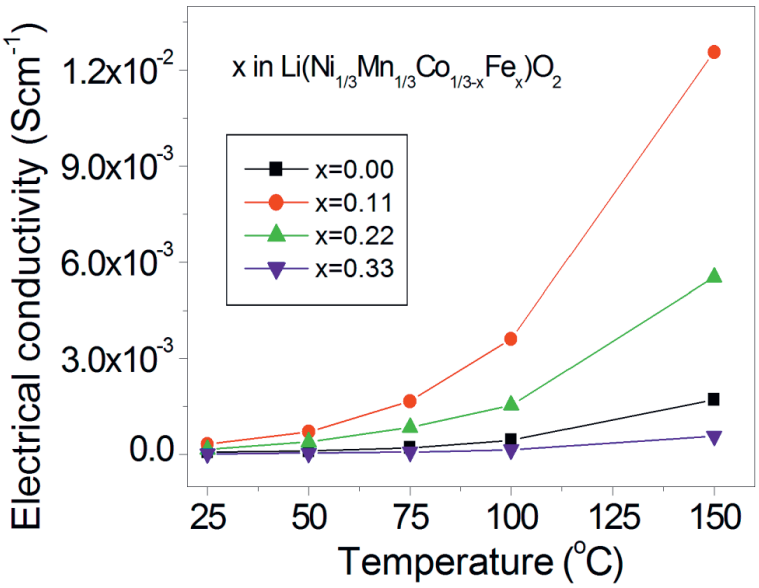

Figure 6.14 *Electrical conductivity of* $Li(Ni_{1/3}Mn_{1/3}Co_{1/3-x}Fe_x)O_2$.

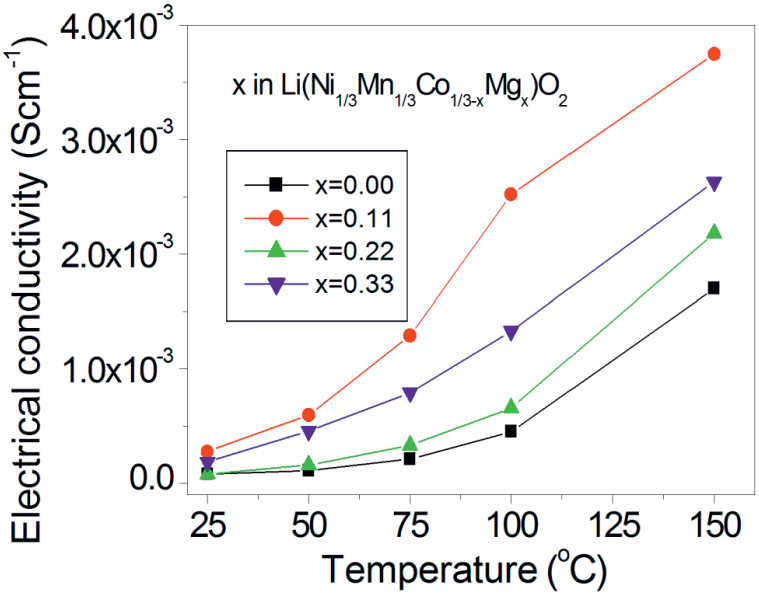

Figure 6.15 *Electrical conductivity of* $Li(Ni_{1/3}Mn_{1/3}Co_{1/3-x}Mg_x)O_2$.

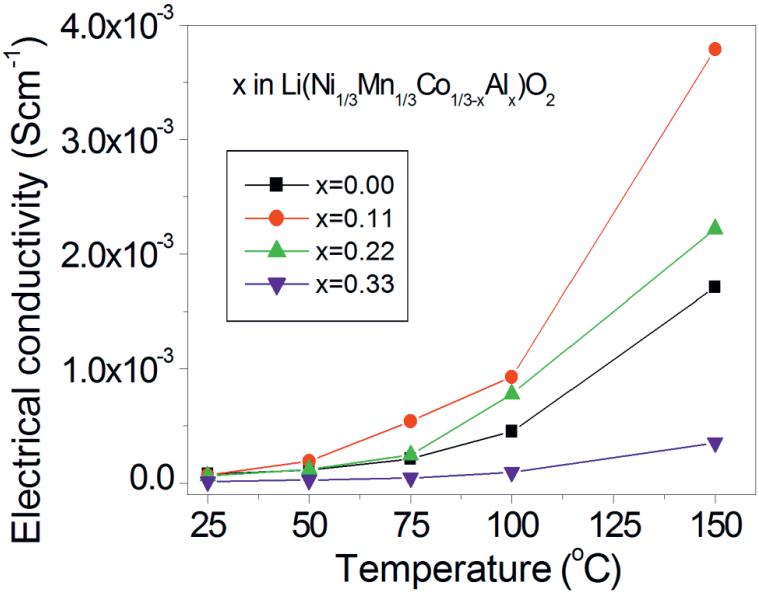

Figure 6.16 *Electrical conductivity of* $Li(Ni_{1/3}Mn_{1/3}Co_{1/3-x}Al_x)O_2$.

Morphology (SEM), upon substitution of Co with other elements [$Li(Ni_{1/3}Mn_{1/3}Co_{1/3-x}M_x)O_2$ M = Al, Mg, Fe and x = 0.11, 0.22, 0.33] is presented in Figure 6.17. The SEM pictures show that the powder materials are sponge-like agglomerates with well-defined, compact and submicron size primary particles. Further, the powders consist of particles in the form of a smoothly edged polyhedron and spherical particles. However, as quite evident from the SEM pictures in all the three compositions where all the Co is substituted by Fe, Al, and Mg (x = 0.33) the smoothly edged polyhedron has become distorted, Figure 6.12. Upon substitution of Mg^{2+} for Co^{3+}, in $Li(Ni_{1/3}Mn_{1/3}Co_{1/3-x}Mg_x)O_2$ at x = 0.33, the layered structure has collapsed due to higher ionic radius of Mg^{2+}, compared to Co^{3+}. This is evident from the SEM picture (M = Mg, x = 0.33), Figure 6.17.

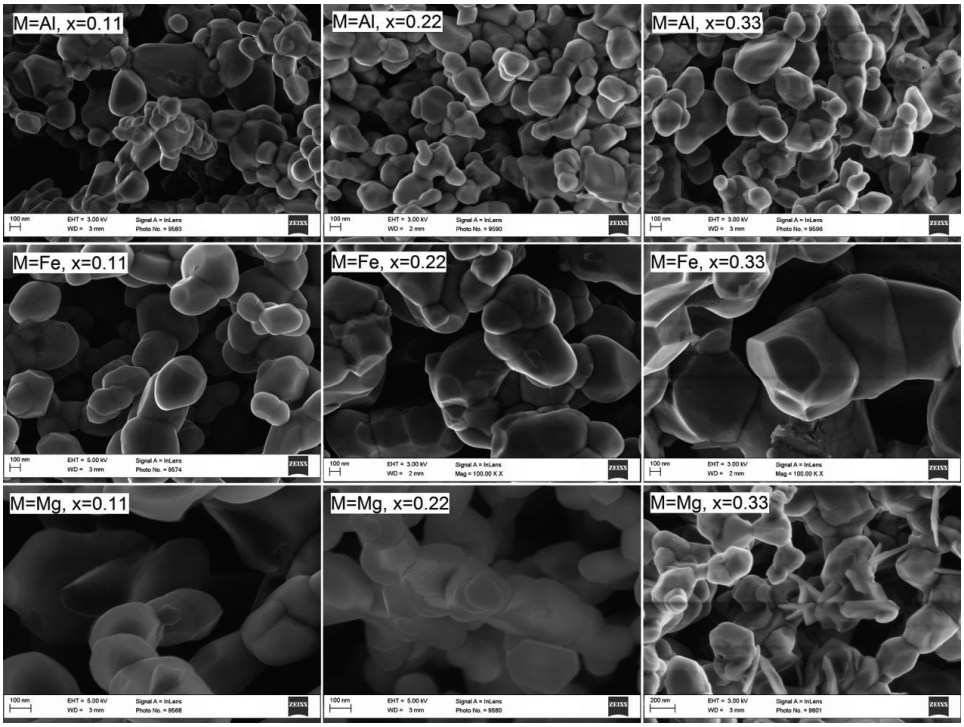

Figure 6.17 *SEM micrographs of $Li(Ni_{1/3}Mn_{1/3}Co_{1/3-x}M_x)O_2$. Sample information is given in the pictures.*

These Fe, Al and Mg substituted NMC materials, [i.e $Li(Ni_{1/3}Mn_{1/3}Co_{1/3-x}M_x)O_2$, *M* = Fe, Al and Mg] give some attractive results, specially x = 0.11 and 0.22 of materials where Co was substituted by Fe and Al, and x = 0.11 material where Co was substituted by Mg. These materials show a considerably higher first cycle charge capacity than the state-of-art cathode material $LiCoO_2$ of LIB (see Table 6.4). Undesirably, the first cycle irreversible capacities are also considerably higher. Matsumura *et al* [113] have reported that the irreversible capacity loss of LIB is related to both the solvent decomposition and the reaction of Li with active sites in the bulk of the carbon electrode. Therefore, one of the reasons for this irreversible capacity of the materials in the present study may be due to the oxidation of the solvents in the electrolyte. It is reasonable to assume that even the substituents might have catalysed the oxidation of the electrolyte, specially taking the ability of iron and its oxides to act as catalysts in to the account. Lately, Xu *et al* [114] have reported that lithium bis(oxalato)borate (LiBOB) based electrolyte has performed better than the popular lithium hexafluorophosphate ($LiPF_6$) based electrolytes, even at temperatures as high as 60 °C, where $LiPF_6$ based electrolytes would usually fail. Consequently, if an electrolyte which is not based on $LiPF_6$ could be developed to be used in the new materials explored in this study, it would be of great interest for production of low cost, environmental friendly lithium ion battery with a higher capacity.

Table 6.4 Comparison of first cycle charge capacity, first cycle discharge capacity and first cycle irreversible charge capacity of $Li(Ni_{1/3}Mn_{1/3}Co_{1/3-x}M_x)O_2$ (M = Fe, Al, Mg and x = 0.11, 0.22, 0.33) materials with those of $LiCoO_2$; charge and discharge rates C/5 ($\sim$ 36 mAh g^{-1}).

M	x	First cycle		
		charge capacity (mAh g^{-1})	discharge capacity (mAh g^{-1})	irreversible charge capacity (mAh g^{-1})
Fe	0.11	179.07	122.24	56.83
	0.22	202.13	101.55	100.58
	0.33	47.15	9.93	37.22
Al	0.11	162.7	119.95	42.75
	0.22	150.34	98.36	51.98
	0.33	119.63	67.67	51.96
Mg	0.11	259.83	125.7	55.12
	0.22	9.3	0.5	8.8
	0.33	1.98	0.19	1.79
$LiCoO_2$		147.31	128.28	19.03

This work on Fe, Al and Mg substituted NMC compositions is reported in paper III.

6.3 Rutile and Columbite structured materials (1D cathode materials)

Rutile and columbite structured materials have a tunnel structure similar to $LiFePO_4$, to which the Li^+ can be inserted and hence have been studied as Li^+ intercalation materials [115,116]. The tunnel structure in rutile (TiO_2) and rutile structured materials is formed by straight chains of edge shared -M^{5+}-M^{2+}-M^{5+}- octahedra along the c axis [paper IV], for example $CrTa_2O_6$. Columbite structured materials on the other hand consist of one -M^{2+}-M^{2+}-M^{2+}- and two -M^{5+}-M^{5+}-M^{5+}- zig-zag chains along the c axis with the chains linked by corner sharing of octahedra, and hence the tunnel structure is also zig-zag compared to the straight tunnels in the rutile structure. Due to this tunnel structure, these materials are also called one dimensional (1D) electrode materials similar to $LiFePO_4$.

Columbite structured materials MNb_2O_6 (*M* = Mn, Co, Ni, Cu, Zn, Cd, Ca, Mg) have previously been studied as Li^+ intercalation materials [117-119]. However, columbite structured $FeNb_2O_6$ has not yet been reported as a Li^+ intercalation material. Neither has the rutile structured $CrNb_2O_6$ material. The present study reports on reversible Li^+ intercalation into the 1D columbite structured $FeNb_2O_6$ and rutile structured $CrNb_2O_6$ materials for the first time.

The terminology used to identify the materials in paper IV is used here as well. $FeNb_2O_6$ was treated 12 h at 900 °C, (Fe-S1) and 1050 °C, (Fe-S2); and $CrNb_2O_6$ was treated at 1050 °C for 12 h, (Cr-S1). PXRD ($CuK\alpha_1$) profiles, Figure 6.18, show that the resultant patterns are in agreement with the reference patterns (PDF numbers are mentioned in the figure) for columbite and rutile structures. However, $FeNb_2O_6$ treated at 1050 °C (Fe-S2) contain $Nb_{12}O_{29}$ type impurity phase [120]. Nevertheless, presence of this impurity does not lead to reduction in the amount of Li^+ inserted into the material as the impurity itself takes part in the Li^+ intercalation process.

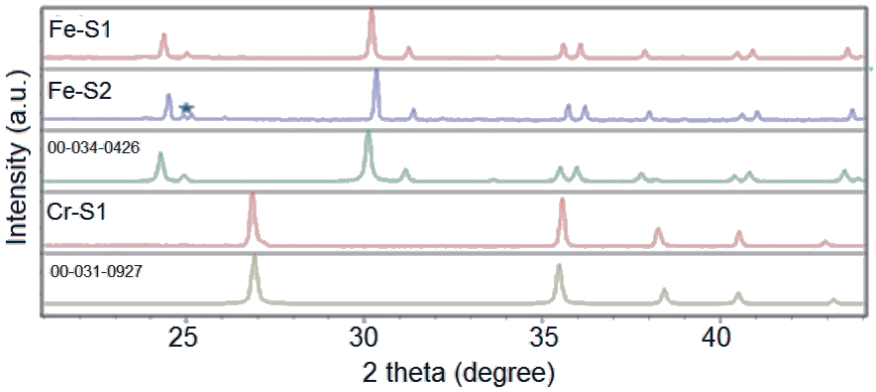

Figure 6.18 *PXRD (CuKα_1) of the columbite and rutile structured materials together with the reference patterns, star represents $Nb_{12}O_{29}$.*

Galvanostatic charge-discharge curves and cyclic voltammograms for all three samples are identical and examples are shown in Figures 6.19 and 6.20, respectively. There are three visible separate discharge plateaus; P1, P2 and P3 in Figure 6.19. Relevant redox peak pairs can be seen in Figure 6.20 (R1, R2, R3-reduction peaks and Ox1, Ox2, Ox3-oxidation peaks). The peak pairs can be assigned to $Nb^{5+/4+}$, $Nb^{4+/3+}$ and $Nb^{3+/2+}$ redox couples. Moreover, there is evidence for Cr taking part in the electrochemical activity in the $CrNb_2O_6$ sample. This is represented by the redox peak pair R4/Ox4, and the redox couple $Cr^{2+/3+}$ is assigned for this peak pair, Figure 20. Hence, this suggests that the oxidation state of Cr in as prepared sample is +3. On the other hand, Fe in $FeNb_2O_6$ does not take part in electrochemical activity suggesting that Fe is in the +2 oxidation state for as prepared samples. These observations on Cr and Fe oxidation states in as prepared samples are further confirmed by the magnetic measurements. In columbite and rutile type AB_2O_6 structures initial Li^+ intercalation step is in general partially irreversible, Figure 6.19. This is because some of the first inserted Li^+ are blocking the tunnel structure. The amounts of Li^+ reversibly inserted in to Fe-S1, Fe-S2 and Cr-S1 (0.47, 0.28 and 0.17 moles) are comparable to insertion of 0.27, 0.26, and 0.7 moles of Li^+ per mole of $MgNb_2O_6$, $CaNb_2O_6$ and $LiNb_2O_6$ [121].

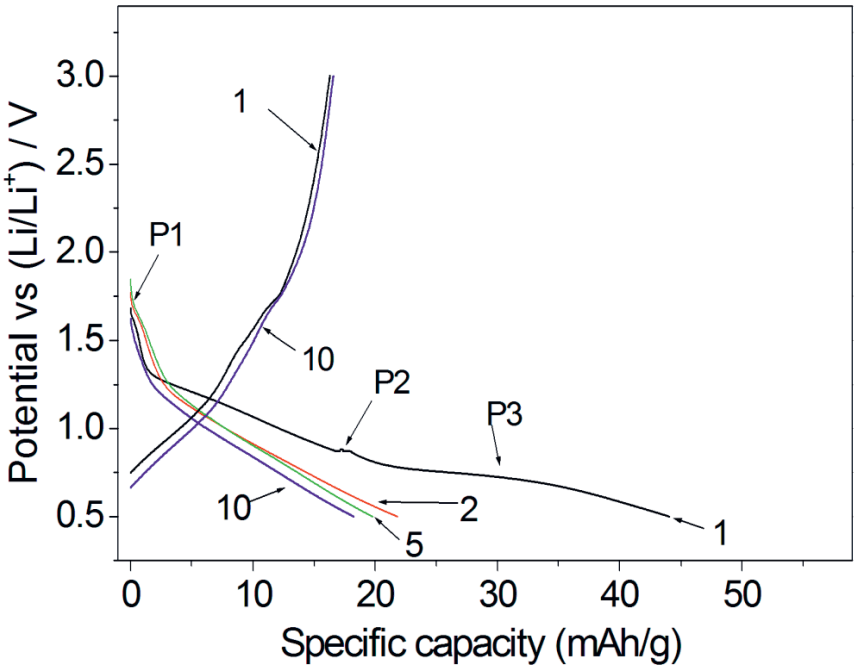

Figure 6.19 *Galvanostatic charge- discharge curves (1, 2, 5, 10) of $CrNb_2O_6$ (Cr-S1); P1,P2,P3 – discharge plateaus.*

SEM pictures of the samples, Figure 6.21, show that the Cr-S1 and Fe-S1 have more or less similar particle sizes, ~ 1 μm while Fe-S2 has a much larger particle size, ~ 4 μm. However, Fe-S1, which is low temperature treated material also contains some ~ 200 nm smaller particles spread among the larger particles as can be seen in Figure 6.21(b). This is very similar to the situation of $LiNi_{0.5-x}Mn_{1.5+x}O_4$ (x = 0.1) materials discussed under section 6.1.2.1, see also Figure 6.10. Among the three studied samples, Fe-S1 shows the highest amount of reversible Li intercalation, close to 55 %, from second cycle. The higher percentage of Li^+ intercalation in Fe-S1 can mainly be attributed to the smaller particle size of the material caused by lower sintering temperature compared to Fe-S2 or Cr-S1 samples. Sintering at a lower temperature results in less dense and smaller crystallites and therefore also a higher surface area.

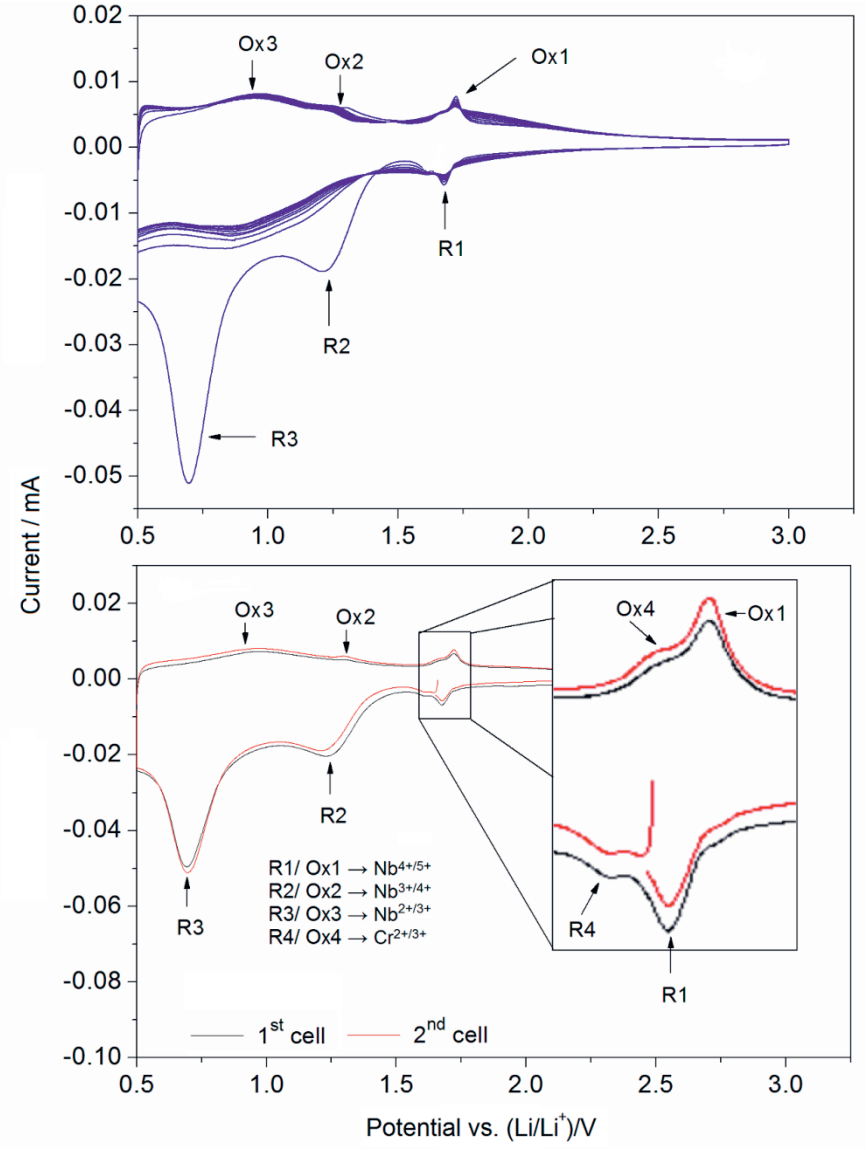

Figure 6.20 *Cyclic voltammograms of* $CrNb_2O_6$ *(Cr-S1).*

If the Li^+ was able to move down the tunnels, the surface area (smaller surface area due to larger particle size) would not affect the amount of Li^+ inserted. However, if the Li^+ becomes immobile close to the openings of the tunnels, then having more openings

(smaller particle size, larger surface area) leads to insertion of more Li^+. Reddy *et al* [122] have demonstrated this phenomenon for columbite type $LiNb_3O_8$. Micrometer sized crystallites showed initial discharge capacity of 234 mAh g^{-1}, however, the value rapidly dropped to 45 mAh g^{-1} for subsequent cycles. In contrast, nanosized $LiNb_3O_8$ showed a reversible capacity of 145 mAh g^{-1} up to the 50^{th} cycle [122]. Post galvanostatic structure analysis by XRD ($CuK\alpha_1$) showed that there was no structural changes taken place during the cell cycling. Initial phase has been retained after the cycling experiments.

Figure 6.21 *SEM micrographs of* ***(a)*** *Cr-S1,* ***(b)*** *Fe-S1and* ***(c)*** *Fe-S2.*

The theoretical capacity for these compounds, assuming a three electron transfer process to reduce the Nb^{5+} to Nb^{2+} (in total six electrons for the two Nb in each formula unit), is 476 mAh g^{-1} for $FeNb_2O_6$ and 481.74 mAh g^{-1} for $CrNb_2O_6$. If nano scale particles of these compounds are obtained, it is possible to reach close to theoretical capacity of the materials. Hence, these would be attractive materials as lithium ion battery cathode materials. It should be mentioned that optimized cathodes could not be prepared in the same manner as for the spinel and substituted NMC materials. A possible reason might have been insufficient mixing with conductive carbon due to the higher density of the current cathode material.

The work on columbite and rutile structured materials is reported in paper IV.

7. CONCLUDING REMARKS

Even though much work has been carried out on various lithium ion battery cathode materials, there is still room for improvements, alternative approaches and deeper insight. The current work has tried to address such issues by new findings and improvements for the cathode materials: spinel $LiNi_{0.5}Mn_{1.5}O_4$, substituted NMC compounds and rutile and columbite structured materials.

For example, *disordered* phase of the spinel materials can be prepared by heat treating at 600 °C for 20h. We also open for the possibility of another red-ox couple, than $Ni^{3+/4+}$, taking part in electrochemistry during final stages of charge-discharge cycles of *disordered* variant.

In this work, powders of various $LiNi_{0.5}Mn_{1.5}O_4$ phases were successfully synthesized by the Pechini method. Furthermore, Raman analysis of the materials appears as an efficient means to distinguish between *ordered* and *disordered* variants of the spinel like material. Raman analysis revealed the existence of *disordered* materials crystallizing in the F*d*-3*m* space group for samples prepared at 600 °C, whereas Ni-Mn cation *ordered* structures described in the $P4_332$ space group for other heat treatment temperatures ranging from 700 - 1000 °C. Powder neutron diffraction data further corroborate the observations of the Raman analysis. Existence of nano-sized particles for powders of $LiNi_{0.5}Mn_{1.5}O_4$ is evident for samples heat treated at 600 and 700 °C (sizes ~10 and ~50 nm, respectively). Propylene Carbonate was used in a successful manner to optimize the performance of the spinel cathode material. The optimized cathodes show a capacity of 137 mAh g^{-1} in contrast to 118 mAh g^{-1} for the normal cathode. This work shows that PXRD (Cu$K\alpha_1$) is not sufficient for determining the phase purity of these spinel materials. There is a possibility of co-existence of *ordered* and *disordered* phases according to refinements on powder neutron diffraction data. *Ordered* phase of $LiNi_{0.5}Mn_{1.5}O_4$ spinel proved to have superior structural and electrochemical reversibility in contrast to prior reports. *In-situ* synchrotron cell studies (PXRD, λ= 0.50480 Å and XAS) suggests that the

ordered phase go through two phase changes leading to three separate cubic phases. The three phases correspond to $Ni^{2+}/Ni^{3+}/Ni^{4+}$ rich materials. Nevertheless, the *disordered* phase seemingly shows only one phase transition and the Ni^{3+} to Ni^{4+} oxidation is absent according to Ni K-edge XANES. This means that another redox couple, presumably $Mn^{4+/5+}$, contribute to the charge capacity of the *disordered* materials. However, more detailed studies are needed to confirm this assumption.

The study on substituted NMC compounds revealed the ability of synthesizing fine powders of $Li(Ni_{1/3}Mn_{1/3}Co_{1/3-x}M_x)O_2$, ($M$ = Mg, Fe, Al and x = 0 to 0.33) by the Pechini method with appropriate particle morphology for lithium ion battery. The phase analysis showed formation of appropriate $Li(Ni_{1/3}Mn_{1/3}Co_{1/3})O_2$, solid solutions of R-3*m* crystal structure (α-$NaFeO_2$ layered structure) for x = 0.11 substitution of Fe and Mg. Further, these Fe and Mg substituted materials showed considerably higher room temperature electrical conductivity than the base material $Li(Ni_{1/3}Mn_{1/3}Co_{1/3})O_2$ (over 0.9 $x10^{-5}$ S/cm at 25 °C). In the cell studies, Fe and Mg substituted compositions with x = 0.11, showed a specific capacity of 122 and 125 mAh g^{-1}, respectively. They are comparable to the specific capacity of the state of the art $LiCoO_2$ cathode material. Overall, this study revealed the possibility of preparing $Li(Ni_{1/3}Mn_{1/3}Co_{1/3-x}M_x)O_2$, ($M$ = Mg, Fe, Al and x = 0 to 0.33) materials with appropriate structural and electrochemical properties suitable for the lithium ion battery cathode.

The possibility for reversible lithium insertion into columbite and rutile structured $FeNb_2O_6$ and $CrNb_2O_6$ was proven for the first time. The results show comparable amount of Li insertion to other AB_2X_6 materials investigated previously. All samples studied showed signs of blocking, which means that the routes to increase performance by nano-structuring will be essential if these materials are to reach the theoretical capacity of 476 mAh g^{-1} for $FeNb_2O_6$ and 482 mAh g^{-1} for $CrNb_2O_6$. If the theoretical capacity could be reached then these materials would become attractive for use in Li ion batteries. Expanding the diffusion paths from 1D tunnels to 2D type by utilizing

structures with some framework Li may prove useful in increasing the reversibility. XRD analysis of electrochemically cycled materials showed that the initial columbite and rutile structures are retained after cycling.

At present there is an unprecedented demand for development of new materials for lithium ion batteries, that can deliver increased capacity, energy density, power density, safety and be environmentally benign as well. Although all three components; cathode, anode and electrolyte are important, much attention is given on developing better cathode materials. Therefore, strategies are needed for engineering alternatives to the prominent cathode material ($LiCoO_2$). Exploration of possible nano structured materials and nano composites is also an option to achieve these goals. The current work has shown that it is possible to obtain deeper insight into assumed well known materials, such as $LiNi_{0.5}Mn_{1.5}O_4$, using suitable tools. We have thereby questioned the previously accepted assumptions with respect to importance of order and disorder in cationic distributions. Moreover, we have shown ability to study materials that previously were not possible to characterize electrochemically, by using proper electrode preparation techniques, examples $FeNb_2O_6$ and $CrNb_2O_6$. The current findings point at the importance of continuously revisiting known systems with better tools, in addition to exploring new compounds as replacements for technologically important materials, in this case, cathode materials for lithium ion batteries. The path for narrowing the gap towards gasoline in energy density is long, and every small step is required.

REFERENCE

[1] Pancaldi G., Notes Rec. R. Soc. 2009, 63, 247.

[2] Scherson, D.A., Palencsar, A., *Interface, The Electrochemical Society*, 2006**,** 15, 19.

[3] *Handbook of batteries*, Third edition (ed. D. Linden and T.B. Reddy), McGraw-Hill (2002).

[4] Samarasingha P., Tran-Nguyen D., Behm M. and Wijayasinghe A., *Electrochimica Acta*, 2008, 53, 7995.

[5] *Advances in Lithium-Ion Batteries* (ed. Schalkwijk W.A.V and Scrosati B.) Kluwer Academic Publishers (2002).

[6] Goodenough J.B., Kim Y., *Chem. Mater.*, 2010, 22, 587.

[7] Dunn, B., Kamath, H., Tarascon, J.M., *Science*, 2011,334, 928.

[8] Islam, M.S., Fisher, C.A.J, *Chem. Soc. Rev.*, 2014,43, 185.

[9] Whittingham, M. S., *Chemical reviews*, 2004**,** 104, 4271.

[10] Ohzuku T., Brodd R.J., *J. Power Sources*, 2007, 174, 449.

[11] Whittingham, M. S., *J. Electrochem. Soc.,* 1975, *122*, 526.

[12] Liang, C. C., Bolster, M. E.; Murphy, R. M., *U.S. Patents* 4,310,609 , 1982.

[13] Takeuchi, E. S., Thiebolt, W. C., *J. Electrochem. Soc.* 1988, *135*, 2691.

[14] Wu,Y., Zhu, P., Zhao, X., Reddy, M.V., Peng, S., Chowdari, B.V.R., Ramakrishna, S., *J. Mater. Chem., A*, 2013,1, 852.

[15] Broadhead, J., *U.S. Patent* 3,791,867, 1973.

[16] Trumbore, F. A., *Pure & Appl. Chem.,* 1979, 5*2*, 119.

[17] Huggins, R.A., *Advanced Batteries : Materials Science Aspects, Springer (ISBN: 978-0-387-76423-8 , 2009.*

[18] Armand, M. B., *U.S. Patent* 4,041,220, 1977.

[19] Gunst, S., Klein, A., Jaegermann, W., Tomm, Y., Crawack, H.J., Jungblut, H., *Ionics*, 2000,6,180.

[20] Whittingham, M. S., *U.S. Patent* 4009052, 1977.

[21] Gamble, F. R., Osiecki, J. H., Cais, M., Pishardy, R., Disalvo, F. J., Geballe, T. H., *Science,* 1971, *174*, 493.

[22] Gamble, F. R., Thompson, A. H., *Solid State Commun.,* 1978, *27*, 379.

[23] Holleck, G. L., Driscoll, J. P., *Electrochim. Acta,* 1977, *22*, 647.

[24] Thompson, A. H., *Phys. Rev. Lett.,* 1975, *35*, 1786.

[25] Whittingham, M. S., *J. Electrochem. Soc.,* 1976, *123*, 315.

[26] Nuspl, G., Yoshizawa, K., Yamabe, T., *J. Mater. Chem., 1997*, 7, 2529.

[27] Murphy, D. W., *U.S. Patents* 4035555, 1977.

[28] Gamble, F. R., Thompson, A. H., *Solid State Commun.,* 1978, *27*, 379.

[29] He, P., Yu, H., Li, D., Zhou, H. , *J. Mater. Chem.*, 2012,22, 3680.

[30] Dampier, F. W., *J. Electrochem. Soc.* 1974, *121*, 656.

[31] Wang, X.J., Nesper, R., Villevielle, C., Novak, P., *Advanced Energy Materials*, 2013,3,606.

[32] Delmas, C., Cognac-Auradou, H., Cocciantelli, J. M., Me´ne´trier, M., Doumerc, J. P., *Solid State Ionics,* 1994, *69*, 257.

[33] Aurbach, D., Gamolsky, K., Markovsky, B., Salitra, G., Gofer, Y., Heider, U., Oesten R., Schmidt, M., *J. Electrochem. Soc.*, 2000, 147, 1322.

[34] Andersson, A.M., Abraham, D.P., Haasch, R., MacLaren, S., Liu J., Amine, K., *J. Electrochem. Soc.*, 2002, 149, A1358.

[35] Chebiam, R.V., Prado F., Manthiram, A., *Chem. Mater.*, 2001, 13, 2951.

[36] Amatucci, G. G., Tarascon, J. M., Klein, L. C. *J. Electrochem. Soc.,* 1996, 143, 1114.

[37] Rossen, E., Reimers, J. N., Dahn, J. R., *Solid State Ionics,* 1993, 62, 53.

[38] Gabrisch, H., Yazimi, R., Fultz, B., *J. Electrochem. Soc.,* 2004, 151, A891.

[39] Johnson, A.P., Schlaikjer, C.R., *J. Power Sources,* 1997, 68, 402.

[40] Ozawa, K., *Solid State Ionics,* 1994, 69, 212.

[41] Goodenough, J. B., Mizuchima, K., *U.S. Patent* 4,302,518, 1980.

[42] Goodenough, J. B., Mizushima, K., *U.S. Patent* 4,357,215, 1981.

[43] Dahn, J. R., Sacken, U. V., Michal, C. A., *Solid State Ionics,* 1990, *44*, 87.

[44] Chen, R., Whittingham, M. S., *J. Electrochem. Soc.,* 1997, *144*, L64.

[45] Chen, R., Chirayil, T., Whittingham, M. S., *Solid State Ionics,* 1996, *86*, 1.

[46] Numata, K., Yamanaka, S., *Solid State Ionics,* 1999, *118*, 117.

[47] Ngala, J.K., Chernova, N.A., Ma, M., Mamak, M., Zavalija, P.Y., Whittingham, M.S., *J. Mater. Chem.,* 2004, *14*, 214.

[48] Nitta, Y., Okamura, K., Haraguchi, K., Kobayashi, S., Ohta, A., *J. Power Sources,* 1995, 54, 511.

[49] Caurant, D., Baffier, N., Bianchi, V., Gre´goire, G., Bach, S., *J. Mater. Chem.,* 1996, 6, 1149.

[50] Rossen, E., Jones, C. D. W., Dahn, J. R., *Solid State Ionics,* 1992, 57, 311.

[51] Spahr, M. E., Nova´k, P., Schnyder, B., Haas, O., Nesper, R., *J. Electrochem. Soc.,* 1998, 145, 1113.

[52] Yue, P., Wang, Z., Peng, W., Li, L., Chen, W., Guo, H., Li, X., *J. Powder Technology,* 2011, 214, 279.

[53] Li, D., Muta, T., Zhang, L., Yoshio, M., Noguchi, H., *J. Power Sources*, 2004, 132,150.

[54] Liu, D., Wang, Z., Chen. L., *Electrochimica Acta,* 2006, 51, 4199.

[55] Liu, Z., Yu, A., Lee, J. Y., *J. Power Sources,* 1999, *82*, 416.

[56] Yoshio, M., Noguchi, H., Itoh, J. I., Okada, M., Mouri, T., *J. Power Sources,* 2000, 90, 176.

[57] Ohzuku, T., Makimura, Y., *Chem. Lett.,* 2001, 642.

[58] Thirunakaran, R., Ramesh Babu, B., Kalaiselvi, N., Kalaiselvi, N., Periasamy, P., Kumar, T.P., Renganathan, N. G., Raghaven, M., Mumiyandi, N., *Bull. Mater. Sci.,* 2001, 24, 51.

[59] Kawai, H., Nagata, M., Tabuchi, M., Tukamoto, H., West, A. R., *Chem. Mater.,*1998, 10, 3266.

[60] Shigemura, H., Sakaebe, H., Kageyama, H., Kobayashi, H., West, A. R., Kanno, R., Morimoto, S., Nasu, S., Tabuchi, M., *J. Electrochem. Soc.*, 2001*,* 148, A730.

[61] Ein-Eli, Y., Howard, Jr. W.F., Lu, S.H., Mukerjee, S., McBreen, J., Vaugheg, J.T., Tackeray, M.M., *J. Electrochem. Soc.,* 1998*,* 145, 1238.

[62] Sun, Y. -K., Hong, K.J., Prakash. J., *J. Electrochem. Soc.,* 2003, 150, A970.

[63] Guan, D., Wang, Y., *Ionics*, 2013, 19, 1.

[64] Padhi, A.K., Nanjundaswamy, K.S., Goodenough, J.B., *J. Electrochem. Soc.*, 1997, 144, 1108.

[65] Andersson A.S., Thomas, J.O., *J. Power Sources*, 2001, 97, 498.

[66] Yang, S., Song, Y., Ngala, K., Zavalij, P. Y., Whittingham, M. S., *J. Power Sources*, 2003, 119, 239.

[67] Ravet, N., Goodenough, J.B., Besner, S., Simoneau, M., Hovington, P., Armand, M., *Abstract #127, 196th Meeting of the Electrochemical Society*, Hawaii,Oct. (1999).

[68] Huang, H., Yin, S. C., Nazar, L.F., *Electrochem. Solid-State Lett.*, 2001, 4, A170.

[69] Dominko, R., Bele, M., Gabarscek, M., Remskar, M., Hanzel, D., Pejovnik, S., Jannik, J., *J. Electrochem. Soc.*, 2005, 152, A607.

[70] Yamada, A., Chung, S.C., Hinokuma, K., *J. Electrochem. Soc.*, 2001, 148, A224.

[71] Yang, S. Zavalij, P.Y., Whittingham, M.S., *Electrochem. Comm.*, 2001, 3, 505.

[72] Prosini, P.P., Carewska, M., Scaccia, S., Wisniewski, P., Passerini S., Pasquali, M., *J. Electrochem. Soc.*, 2002, 149, A886.

[73] Nytén, A., Abouimrane, A., Armand, M., Gustafsson, T., Thomas, J.O., *Electrochem. Comm.*, 2005, 7, 156.

[74] Lee, K.T., Lytel, J.C., Ergang, N.C., Oh, S.M., Stein, A., *Adv.Func.Mater.,*2005,15, 547.

[75] Dey, A.N., *J. Electrochem. Soc.*, 1971, 118, 1547.

[76] Huggins, R.A., *Handbook of Battery Materials (ed. J.O. Besenhard)*, Wiley-VCH, Weinheim (1999).

[77] Vaughey, J.T., Johnson, C.S., Kropf, A.J., Benedek, R., Thackeray, M.M., Tostman, H., Sarakonsri, T., Hackney, S., Fransson, L., Edström, K., Thomas, J.O., *J. Power Sources*, 2001, 97, 194.

[78] Larcher, D., Beaulieu, L. Y., MacNeil, J. R. Dahna, D. D., *J. Electrochem. Soc*., 2000, 147, 1658.

[79] Fransson, L.M.L., Vaughey, J.T., Edström, K., Thackeray, M.M., *J. Electrochem. Soc*., 2003, 150, A86.

[80] Tarascon J.-M., Armand, M., *Nature*, 2001, 414, 359.

[81] Kerr, J.B., Han, Y.B., Liu, G., Reeder, C., Xie, J., *Electrochim. Acta*, 2004, 50,235.

[82] Stura, E., Nicolini, C., *Analytica Chimica Acta*, 2006, 568, 57.

[83] Aifantis, K.E., Dempsey, J.P., *J. Power Sources,* 143, 2005, 203.

[84] Maier, J., *Nat. Mater,* 2005**,** 4, 805.

[85] Arico, A. S., Bruce, P., Scrosati, B., *Nat. Mater,* 2005, 4, 366.

[86] Zhou, H. S., Li, D. L., Hibino, M. & Honma, I., *Angew. Chem. Int. Ed.,* 2005**,** 44, 797.

[87] West, A. R., *Solid State Chemistry.* John Wiley & Sons Ltd.: Redwood Books, 1997.

[88] Huang, X., Zhang, Q., Gan, J., Chang, H., Yang, Y., *J. Power Sources,* 2011, 158, A139.

[89] Shaju, K.M., Subba Rao, G.V., Chowdari, B.V.R., *Electrochimica Acta,* 2002, 48, 145.

[90] Choy, J.H., Kim, D.H., Kwon, C.W., Hwang, S.J., Kim, Y.I., *J. Power Sources,* 1999,77,1.

[91] Wu, X.M., Li, X.H., Xiao, Z.B., Liu, J.B., Yan, W.B., Ma, M.Y., *Mater. Chem. Phys.,* 2004, 84.

[92] Bao, S.J., Liang, Y.Y., Li, H.L., *Materials Letters,* 2005, 59, 3761.

[93] Wijayasinghe, A., Bergman, B., Lagergren, C., *Solid State Ionics,* 2006**,** 177, 165.

[94] Zhu, C., Akiyama, T., *Electrochimica Acta,* 2014, 127, 290.

[95] Pechini, M.P., *US Patent* 3,330,697, 1967.

[96] David R. Lide, ed., CRC *Handbook of Chemistry and Physics*, Internet Version 2005, <http://www.hbcpnetbase.com>, CRC Press, Boca Raton, FL, 2005.

[97] Stoyanova, R., Zhecheva, E., *Journal of Solid State Chemistry*, 1994, 108, 211.

[98] L. Koester, H. Rauch, and E. Seymann, *Atomic data and nuclear data tables,* 1991, 49, 65-120, Academic press, Inc.

[99] Kim, J.H., Myung, S.T., Yoon, C.S., Kang, S.G., Sun, Y.K., *Chem. Mater.*, 2004, 16, 906.

[100] Shaju, K.M., and Bruce, P.G., *Dalton Trans.,* 2008, 5471.

[101] Carvajal, J.R., Laboratoire Léon Brillouin, *Fullprof 2k, Version 2.05*, 2011.

[102] Larson, A.C., and Von Dreele, R.B., *Los Alamos National Laboratory report* 2004, *LAUR*, 86-748.

[103] Cai, Z. Liu, K. An, C. Liang *J. Mater. Chem. A,* 2013, 1, 6908.

[104] Cabana, J., Casas-Cabanas, M., Omenya, F.O., Chernova, N.A., Whittingham, M.S., Grey, C.P., *Chem. Mater.*2012, 24, 2952.

[105] Kim, J. H., Myung, S. T., Yoon, C. S., Kang, S. G., Sun, Y. K., *Chem. Mater*., 2004, 16, 906.

[106] Lee, E., Persson, K. A., *Energy Environ. Sci.* 2012, 5, 6047.

[107] Yi, T.F., Hu, X.G., *J. Power Sources*, 2007,167, 185.

[108] Sun, Y.C., Wang, Z.X., Huang, X.J., Chen, L.Q., *J. Power Sources*, 2004,132, 161.

[109] Okada, M., Lee, Y.S., Yoshio, M., *J. Power Sources*, 2000,90, 196.

[110] Jang, M.W., Jung, H.G., Scrosati, B., Sun, Y.K., *J. Power Sources*, 2012,220, 354.

[111] Stoyanova, R., Zhecheva, E., *J. Solid State Chem.*, 1994, 108, 211.

[112] Hu, S.K., Chou, T.C., Hwang, B.J., Ceder G., *J. Power Sources,* 2006, 160, 1287.

[113] Matsumura, Y., Wang, S., Mondori, J., *J. Electrochemical Society* , 1995, 142, 2914.

[114] Xu, K., Zhang, S., Jow, T.R., Xu, W., Angell, C.A., *Electrochem. Solid-State Lett.,* 2002**,** 5, A26.

[115] Kanamura, K., Yuasa, K., Takehara, Z., *J. Power Sources*, 1987, 20, 127.

[116] Murphy, D.W., Di, S.F.J., Carides, J.N., Waszczak, J.V., *Mater. Res. Bull.*, 1978, 13, 1395.

[117] Martı'nez-de la Cruz, A., Alcaraz, N.L., Fuentes, N.L., Torres-Martı'nez, L.M., *J. Power Sources*, 1999, 81, 255.

[118] Sato, M., Hama, Y., *J. Solid State Chem.*, 1995, 118, 193.

[119] Reddy, M.A., Varadaraju, U.V., *Journal of Physical Chemistry C*, 2011, 115, 25121.

[120] Lufaso, M. W., Woodward, P. M., *Acta Crystallographica Section B ,* 2001, *57*, 725.

[121] Reddy, M. V., Subba Rao, G. V., Chowdari, B. V. R., *Chemical Reviews,* 2013, *113*, 5364.

RESEARCH PUBLICATIONS

Spinel phases (3D cathode materials)

I. Neutron diffraction and Raman analysis of $LiNi_{0.5}Mn_{1.5}O_4$ spinel type oxides for use as lithium ion battery cathode and their capacity enhancements

Authors: Pushpaka B. Samarasingha*, Niels H. Andersen, Magnus Sørby, Susmit Kumar, Ola Nilsen, Helmer Fjellvåg.

Journal: **Manuscript.**

II. Detailed *in-situ* synchrotron study of ordered (*$P4_332$*) and disordered (*Fd-3m*) $LiNi_{0.5}Mn_{1.5}O_4$ spinel lithium ion battery cathode

Authors: Pushpaka B. Samarasingha*, Jonas Sottmann, Serena Margadonna, Ola Nilsen, Helmer Fjellvåg.

Journal: **Manuscript.**

Layered NMC compositions (2D cathode materials)

III. Development of cathode materials for lithium ion rechargeable batteries based on the system $Li(Ni_{1/3}Mn_{1/3}Co_{1/3-x}M_x)_2$, ($M$ = Mg, Fe, Al and x = 0.00 to 0.33)

Authors: Pushpaka B. Samarasingha*, Athula Wijayasinghe, Mårten Behm, Lakshman Dissanayake , Göran Lindbergh.

Journal: *Solid State Ionics*, **268 (2014) 226–230**, DOI - j.ssi.2014.07.012.

Rutile and Columbite structured materials (1D cathode materials)

IV. Investigation of Li^+ insertion in columbite structured $FeNb_2O_6$ and rutile structured $CrNb_2O_6$ materials

Authors **:** Pushpaka B. Samarasingha, Chris I. Thomas*, Helmer Fjellvåg.

Journal: *Electrochimica Acta*, **153 (2015) 232–237,** DOI - j.electacta.2014.12.004.

I

Paper I

Neutron diffraction and Raman analysis of $LiNi_{0.5}Mn_{1.5}O_4$ spinel type oxides for use as lithium ion battery cathode and their capacity enhancements

Pushpaka B. Samarasingha*, Niels H. Andersen, Magnus Sørby, Susmit Kumar, Ola Nilsen and Helmer Fjellvåg

In Manuscript

II

Paper II

Detailed *in-situ* synchrotron study of ordered (*$P4_332$*) and disordered (*Fd*-3*m*) $LiNi_{0.5}Mn_{1.5}O_4$ spinel lithium ion battery cathode

Pushpaka B. Samarasingha*, Jonas Sottmann, Serena Margadonna, Ola Nilsen and Helmer Fjellvåg

In Manuscript

III

Paper III

Development of cathode materials for lithium ion rechargeable batteries based on the system $Li(Ni_{1/3}Mn_{1/3}Co_{1/3-x}M_x)_2$, ($M$ = Mg, Fe, Al and x = 0.00 to 0.33)

Pushpaka B. Samarasingha*, Athula Wijayasinghe, Mårten Behm, Lakshman Dissanayake and Göran Lindbergh

Solid State Ionics, **268 (2014) 226–230**, DOI - j.ssi.2014.07.012

IV

Paper IV

Investigation of Li^+ insertion in columbite structured $FeNb_2O_6$ and rutile structured $CrNb_2O_6$ materials

Pushpaka B. Samarasingha, Chris I. Thomas* and Helmer Fjellvåg

Electrochimica Acta, **153 (2015) 232-237,** DOI - j.electacta.2014.12.004